

# Earth and Space Science

## RESEARCH ARTICLE

10.1029/2024EA003935

### Special Collection:

Observing CO<sub>2</sub> from space: A Decade of progress from NASA's Orbiting Carbon Observatories (OCO-2 and OCO-3)

### Key Points:

- Dry-air mole-fractions of carbon dioxide (X<sub>CO<sub>2</sub></sub>) from the Orbiting Carbon Observatory-2 (OCO-2) are evaluated against ground-based data
- OCO-2 X<sub>CO<sub>2</sub></sub> data show absolute average biases no greater than 0.20 ppm against the Total Carbon Column Observing Network (TCCON) globally
- OCO-2's land nadir/glint mode outperforms other observation modes when compared to TCCON, with a bias value of  $-0.03 \pm 0.85$  ppm

### Supporting Information:

Supporting Information may be found in the online version of this article.

### Correspondence to:

S. Das,  
saswati.das@jpl.nasa.gov

### Citation:

Das, S., Kiel, M., Laughner, J., Osterman, G., O'Dell, C. W., Taylor, T. E., et al. (2025). Comparisons of the v11.1 Orbiting Carbon Observatory-2 (OCO-2) X<sub>CO<sub>2</sub></sub> measurements with GGG2020 TCCON. *Earth and Space Science*, 12, e2024EA003935. <https://doi.org/10.1029/2024EA003935>

© 2025 National Institute of Water and Atmospheric Research. Jet Propulsion Laboratory, California Institute of Technology. Karlsruhe Institute of Technology and The Author(s). Government sponsorship acknowledged. Earth and Space Science published by Wiley Periodicals LLC on behalf of American Geophysical Union. This article has been contributed to by U.S. Government employees and their work is in the public domain in the USA. This is an open access article under the terms of the [Creative Commons Attribution License](#), which permits use, distribution and reproduction in any medium, provided the original work is properly cited.

## Comparisons of the v11.1 Orbiting Carbon Observatory-2 (OCO-2) X<sub>CO<sub>2</sub></sub> Measurements With GGG2020 TCCON

Saswati Das<sup>1</sup> , Matthias Kiel<sup>1</sup> , Joshua Laughner<sup>1</sup> , Gregory Osterman<sup>1</sup>, Christopher W. O'Dell<sup>2</sup> , Thomas E. Taylor<sup>2</sup> , Brendan Fisher<sup>1</sup> , Frédéric Chevallier<sup>3</sup> , Nicholas M. Deutscher<sup>4,5</sup> , Manvendra K. Dubey<sup>6</sup> , Dietrich G. Feist<sup>7,8,9</sup> , Omaira Garcia<sup>10</sup> , David W. T. Griffith<sup>5</sup>, Frank Hase<sup>11</sup>, Laura T. Iraci<sup>12</sup> , Rigel Kivi<sup>13</sup> , Isamu Morino<sup>14</sup> , Justus Notholt<sup>4</sup> , Hirofumi Ohyama<sup>14</sup>, David Pollard<sup>15</sup> , Sébastien Roche<sup>16</sup>, Coleen M. Roehl<sup>17</sup>, Constantina Rousogenous<sup>18</sup>, Mahesh Kumar Sha<sup>19</sup> , Kei Shiomi<sup>20</sup>, Kimberly Strong<sup>21</sup> , Ralf Sussmann<sup>22</sup>, Yao Te<sup>23</sup> , Geoffrey Toon<sup>1</sup> , Mihalis Vrekoussis<sup>4,18</sup>, Pucai Wang<sup>24,25</sup>, Thorsten Warneke<sup>4</sup> , Paul Wennberg<sup>17</sup> , Abhishek Chatterjee<sup>1</sup> , Vivienne H. Payne<sup>1</sup> , and Debra Wunch<sup>21</sup> 

<sup>1</sup>Jet Propulsion Laboratory, California Institute of Technology, Pasadena, CA, USA, <sup>2</sup>Colorado State University, Fort Collins, CO, USA, <sup>3</sup>Laboratoire des Sciences du Climat et de l'Environnement/IPSL, Université Paris-Saclay, Gif-sur-Yvette, France, <sup>4</sup>Institute of Environmental Physics (IUP), University of Bremen, Bremen, Germany, <sup>5</sup>University of Wollongong, Wollongong, NSW, Australia, <sup>6</sup>Los Alamos National Laboratory, Los Alamos, NM, USA, <sup>7</sup>Max Planck Institute for Biogeochemistry, Jena, Germany, <sup>8</sup>Lehrstuhl für Physik der Atmosphäre, Ludwig-Maximilians-Universität München, Munich, Germany, <sup>9</sup>Deutsches Zentrum für Luft- und Raumfahrt, Institut für Physik der Atmosphäre, Oberpfaffenhofen, Germany, <sup>10</sup>Izaña Atmospheric Research Center, State Meteorological Agency of Spain (AEMet), Tenerife, Spain, <sup>11</sup>Karlsruhe Institute of Technology (KIT), Institute of Meteorology and Climate Research (IMK-ASF), Karlsruhe, Germany, <sup>12</sup>Atmospheric Science Branch, NASA Ames Research Center, Moffett Field, CA, USA, <sup>13</sup>Finnish Meteorological Institute, Sodankylä, Finland, <sup>14</sup>National Institute for Environmental Studies (NIES), Tsukuba, Japan, <sup>15</sup>National Institute of Water and Atmospheric Research, Lauder, New Zealand, <sup>16</sup>Environmental Defense Fund, New York, NY, USA, <sup>17</sup>California Institute of Technology, Pasadena, CA, USA, <sup>18</sup>Climate and Atmosphere Research Centre (CARE-C), The Cyprus Institute, Nicosia, Cyprus, <sup>19</sup>Royal Belgian Institute for Space Aeronomy, Brussels, Belgium, <sup>20</sup>Earth Observation Research Center (EORC), Japan Aerospace Exploration Agency (JAXA), Tsukuba, Japan, <sup>21</sup>University of Toronto, Toronto, ON, Canada, <sup>22</sup>Karlsruhe Institute of Technology (KIT), Institute of Meteorology and Climate Research (IMK-IFU), Garmisch-Partenkirchen, Germany, <sup>23</sup>CNRS, Sorbonne Universités, Observatoire de Paris, PSL Research University, Paris, France, <sup>24</sup>LAGEO, Chinese Academy of Sciences, the Institute of Atmospheric Physics, Beijing, China, <sup>25</sup>University of Chinese Academy of Sciences, Beijing, China

**Abstract** The Orbiting Carbon Observatory 2 (OCO-2) is NASA's first Earth observation satellite mission dedicated to studying the sources and sinks of carbon dioxide (CO<sub>2</sub>) on a global scale. The observations of reflected sunlight are inverted in a retrieval algorithm to produce estimates of the dry air mole-fractions of CO<sub>2</sub> (X<sub>CO<sub>2</sub></sub>). The OCO-2 Level 2 data release, version 11.1 (v11.1) retrievals from the Atmospheric Carbon Observations from Space (ACOS) algorithm, includes significant improvements in the X<sub>CO<sub>2</sub></sub> data product compared to older OCO-2 data versions. This work compares the v11.1 X<sub>CO<sub>2</sub></sub> from OCO-2 against X<sub>CO<sub>2</sub></sub> estimates collected from a global ground-based network known as the Total Carbon Column Observing Network (TCCON), OCO-2's primary validation source. The OCO-2 project provides a version of the Level 2 data product, called "lite" files that include calibrated and bias-corrected X<sub>CO<sub>2</sub></sub> values, accessible together with all OCO-2 data products through the NASA Goddard Earth Sciences Data and Information Services Center (GES DISC). This work shows that OCO-2 X<sub>CO<sub>2</sub></sub> observations made between September 2014 and December 2023, after quality filtering and the application of an averaging kernel correction, agree well with coincident TCCON data for all OCO-2 observational modes of land (nadir, glint, target) and ocean (glint). The aggregated, bias-corrected, and quality-filtered absolute average bias values are less than or equal to 0.20 parts per million (ppm) globally for all OCO-2 observation modes, where the biases do not indicate a statistically significant time dependence. The land nadir/glint mode has the lowest bias value of  $-0.03 \pm 0.85$  ppm.

**Plain Language Summary** Carbon dioxide (CO<sub>2</sub>) is a major greenhouse gas that contributes to global warming, warranting the continuous monitoring of its concentration in the atmosphere to improve our understanding of the dynamics of climate change and predict future climate scenarios. Satellites play an important role in providing comprehensive global coverage of atmospheric CO<sub>2</sub>, particularly making CO<sub>2</sub> observations possible over remote and inaccessible areas. The OCO-2 (OCO-2) is a NASA mission dedicated to

Received 22 AUG 2024  
Accepted 10 MAY 2025

**Author Contributions:**

**Conceptualization:** Saswati Das,

Matthäus Kiel, Joshua Laughner,

Gregory Osterman, Debra Wunch

**Data curation:** Joshua Laughner,

Frédéric Chevallier, Nicholas

M. Deutscher, Manvendra K. Dubey,

Dietrich G. Feist, Omaira Garcia, David

W. T. Griffith, Frank Hase, Laura T. Iraci,

Rigel Kivi, Isamu Morino, Justus Notholt,

Hirofumi Ohyama, David Pollard,

Sébastien Roche, Coleen M. Roehl,

Constantina Rousogenous, Mahesh

Kumar Sha, Kei Shiomi, Kimberly Strong,

Ralf Sussmann, Yao Té, Geoffrey Toon,

Mihalis Vrekoussis, Pucai Wang,

Thorsten Warneke, Paul Wennberg,

Debra Wunch

**Formal analysis:** Saswati Das,

Matthäus Kiel, Joshua Laughner,

Gregory Osterman

**Investigation:** Saswati Das

**Methodology:** Saswati Das,

Matthäus Kiel, Joshua Laughner,

Gregory Osterman, Christopher

W. O'Dell, Thomas E. Taylor,

Brendan Fisher, Debra Wunch

**Project administration:**

Abhishek Chatterjee, Vivienne H. Payne

**Resources:** Gregory Osterman,

Abhishek Chatterjee, Vivienne H. Payne

**Supervision:** Gregory Osterman

**Validation:** Saswati Das, Matthäus Kiel,

Joshua Laughner, Gregory Osterman

**Visualization:** Saswati Das, Debra Wunch

**Writing – original draft:** Saswati Das,

Matthäus Kiel

**Writing – review & editing:**

Joshua Laughner, Gregory Osterman,

Christopher W. O'Dell, Thomas E. Taylor,

Brendan Fisher, Frédéric Chevallier,

Nicholas M. Deutscher, Manvendra

K. Dubey, Omaira Garcia, David

W. T. Griffith, Frank Hase, Laura T. Iraci,

Rigel Kivi, Isamu Morino, Justus Notholt,

Hirofumi Ohyama, David Pollard,

Sébastien Roche, Coleen M. Roehl,

Constantina Rousogenous, Mahesh

Kumar Sha, Kei Shiomi, Kimberly Strong,

Ralf Sussmann, Yao Té, Geoffrey Toon,

Mihalis Vrekoussis, Pucai Wang,

Thorsten Warneke, Paul Wennberg,

Abhishek Chatterjee, Vivienne H. Payne,

Debra Wunch

studying atmospheric CO<sub>2</sub> with a high degree of precision, accuracy, and comprehension. To ensure continued accuracy, reliability, and confidence in data usage, the new and improved version 11.1 (v11.1) column-averaged dry-air mole fraction of CO<sub>2</sub> (X<sub>CO<sub>2</sub></sub>) product from OCO-2 is validated in this study against the Total Carbon Column Observing Network (TCCON), a global network of ground-based Fourier Transform Spectrometers. The comparisons indicate that aggregated bias-corrected and quality-filtered X<sub>CO<sub>2</sub></sub> estimates from OCO-2 compare well with TCCON, with absolute average biases less than or equal to 0.20 parts per million (ppm) globally.

## 1. Introduction

The Orbiting Carbon Observatory-2 (OCO-2) was launched on 2 July 2014 from the Vandenberg Air Force Base in California, USA. It is NASA's first dedicated satellite mission to measure atmospheric carbon dioxide (CO<sub>2</sub>) and identify its global sources and sinks (Crisp et al., 2004; Crisp & Johnson, 2005). OCO-2 was designed on the heritage of the OCO, which was a mission lost in 2009 due to a malfunction in the launch vehicle and could not reach orbit (Crisp et al., 2008). Its 3-channel, imaging, grating spectrometer collects high-resolution spectra of reflected sunlight in the near-infrared (NIR) and shortwave infrared regions. The sunlight reflected from Earth's surface is collected in three spectral regions centered at 0.765, 1.61, and 2.06 μm. The region centered at 0.765 μm is used to retrieve molecular oxygen (O<sub>2</sub> A-band), and the 1.61 and 2.06 μm bands are the weak and strong CO<sub>2</sub> bands, respectively. The combination of coincident measurements from the three channels is used to produce "soundings" that are analyzed using a "full-physics" retrieval algorithm to produce atmospheric abundances of X<sub>CO<sub>2</sub></sub> and other atmospheric and geophysical quantities such as clouds and aerosol optical depth and distribution, water vapor, temperature, surface pressure, and reflectance, explained in detail in the OCO-2 Data User Guide (OCO-2 DUG, 2023).

The column-averaged dry air mole fraction of atmospheric CO<sub>2</sub> (X<sub>CO<sub>2</sub></sub>) is the ratio of the column abundances of CO<sub>2</sub> and dry air. The altitude-dependent CO<sub>2</sub> number density, when integrated over the atmospheric column, is referred to as the "column abundance." O<sub>2</sub> acts as a suitable proxy for dry air due to its essentially constant mole fraction in dry air (0.2095). The column abundance of dry air is thus estimated using the spectra of the NIR O<sub>2</sub> absorption band. Connor et al. (2008) and O'Dell et al. (2012, 2018) described the optimal estimation retrieval algorithm used to retrieve column abundance of CO<sub>2</sub> from high-resolution spectra of reflected sunlight: the Atmospheric Carbon Observations from Space (ACOS) algorithm, which has been validated extensively (O'Dell et al., 2012, 2018).

X<sub>CO<sub>2</sub></sub> is of paramount importance in carbon cycle science due to its relative insensitivity to vertical mixing and its direct utility in quantifying CO<sub>2</sub> surface fluxes (Byrne et al., 2022; Crowell et al., 2019; Keppel-Aleks et al., 2011; Yang et al., 2007), necessitating its continuous, high-quality measurements. Furthermore, Miller et al. (2007) and Jacobs et al. (2024) assessed that X<sub>CO<sub>2</sub></sub> measurements need to be highly precise (within ±1 ppm, i.e., ~0.25%) and accurate (within ±0.2 ppm, i.e., ~0.05%). This is important to distinguish variations on the order of tenths of a part per million (ppm) well enough against a high background X<sub>CO<sub>2</sub></sub> concentration of approximately 400 ppm (Rayner & O'Brien, 2001; Chevallier et al., 2005, 2014; Miller et al., 2007; Jacobs et al., 2024). OCO-2 has been making highly precise (within 0.3% or 1 ppm) and accurate space-based measurements of X<sub>CO<sub>2</sub></sub> for more than a decade (Eldering et al., 2017), with continuous efforts made by the OCO-2 team toward the improvement of the data quality through the characterization and elimination of biases (Jacobs et al., 2024; Kiel et al., 2019; Mandrake et al., 2015; Taylor et al., 2023; Wunch et al., 2017).

The Total Carbon Column Observing Network (TCCON; Toon et al., 2009; Wunch, Toon, et al., 2011) is the primary source of reference data used to validate OCO-2. TCCON is a global ground-based network that measures X<sub>CO<sub>2</sub></sub> in addition to other atmospheric species and was designated and deployed as the primary validation source for X<sub>CO<sub>2</sub></sub> from OCO-2, the Greenhouse Gases Observing Satellite (GOSAT; Kuze et al., 2009, 2016), the SCanning Imaging Absorption SpectroMeter for Atmospheric CHartographY (SCIAMACHY; Bovensmann et al., 1999), and the Chinese Carbon Dioxide Observation Satellite Mission (TANSAT; Liu et al., 2018). TCCON is a network of solar-viewing ground-based Fourier Transform Spectrometers that records direct solar spectra in the NIR spectral region. These spectra are used to retrieve accurate and precise column-averaged abundance of O<sub>2</sub>, CO<sub>2</sub>, methane (CH<sub>4</sub>), nitrous oxide (N<sub>2</sub>O), hydrofluoric acid (HF), carbon monoxide (CO), water vapor

(H<sub>2</sub>O), and semi-heavy water (HDO). The TCCON instruments, although cannot measure through optically thick clouds, are unaffected by surface properties and are minimally sensitive to aerosols and high cirrus clouds (Keppel-Aleks et al., 2007).

A key aspect of validating X<sub>CO<sub>2</sub></sub> is ensuring that it is tied to the same World Meteorological Organization (WMO) measurement scale as in situ CO<sub>2</sub> data. For OCO-2, this is done vicariously through TCCON. TCCON X<sub>CO<sub>2</sub></sub> data are tied to in situ data through a scale factor derived from comparisons with numerous in situ profiles measured over TCCON sites (Laughner et al., 2024; Messerschmidt et al., 2011; Wunch et al., 2010). OCO-2 data is likewise scaled to match coincident TCCON observations, thus making all three data sets compatible.

In our analysis, the nadir and glint observation modes are combined over land (hereafter, land nadir/glint). The land nadir/glint, ocean glint, and target mode observations from OCO-2 are compared against coincident-TCCON measurements from September 2014 to December 2023. This paper describes the materials and methods in Section 2, the results and discussion in Section 3, and the conclusions in Section 4.

## 2. Materials and Methods

### 2.1. Data Sets

#### 2.1.1. OCO-2

OCO-2 flies at the head of the Earth Observing System Afternoon Constellation (EOS A-Train) and measures using the 3-channel imaging spectrometer over the sunlit hemisphere to record high-resolution spectra of reflected sunlight in the O<sub>2</sub> and CO<sub>2</sub> bands. OCO-2 has a ground-track repeat cycle of 16 days or 233 orbits and measures in three observation modes: nadir, glint, and target. These modes provide data over different surface conditions. The instrument observes pointing straight down at the Earth's surface in the nadir mode. In this mode, the observations provide the best spatial resolution and yield more useful X<sub>CO<sub>2</sub></sub> soundings in partially cloudy or topographically rough regions. Furthermore, the nadir mode is particularly useful for measuring at high latitudes due to shorter paths than the glint mode, which helps reduce aerosol and scattering effects. In the glint mode, the instrument points on the surface at the sun glint spot. The observations made in this mode have higher signal-to-noise ratios (SNR) over dark ocean surfaces. During the first year of making observations, OCO-2's strategy to observe changed to glint-only observations over most of the Pacific and Atlantic oceans and alternating between the nadir and glint modes on all other orbits. The target mode observations are taken primarily for use in validation against ground-based observations from TCCON (Kiel et al., 2019; Wunch, Wennberg, et al., 2011, 2017).

Wunch et al. (2017) published the first validation analysis of OCO-2, using version 7 (v7) data and performing systematic comparisons to TCCON. Since the v7 data product, several major algorithm and calibration changes have been implemented to improve the OCO-2 retrievals. The changes in the OCO-2 version 8 (v8) data product (O'Dell et al., 2018) included the updated radiometric calibration for the L1B product, updated spectrometric parameters, the addition of stratospheric aerosols, and a more pragmatic treatment of the surface reflectance in the L2 algorithm. OCO-2 version 9 (v9) (Kiel et al., 2019) data was released to mitigate topography-related biases in OCO-2 v7 (Wunch et al., 2017) that were also observed in v8. These biases were attributed to relative errors in the surface pressure estimates due to small errors in the pointing of the OCO-2 detector, propagating nearly 1:1 into relative errors in the bias-corrected X<sub>CO<sub>2</sub></sub>. Furthermore, the way the surface pressure a priori value was determined from the meteorological model data affected the surface pressure retrieval. Model results from the GEOS-5 Forward Processing for Instrument Teams (GEOS5 FP-IT) model are used in the OCO-2 retrieval software. It was discovered that a coding error led to incorrect time interpolation while sampling the GEOS5 FP-IT surface pressure results. In v9, significant improvement in how the X<sub>CO<sub>2</sub></sub> data varies with altitude was observed upon using improved geolocation (Kiel et al., 2019) for the eight OCO-2 footprints and resolving the a priori sampling error associated with the meteorological data. The major changes in version 10 (v10) (Taylor et al., 2023) included updates to the L1B calibration to account for radiometric degradation and bad pixel samples. Changes were made to the trace gas spectroscopic parameters used in the retrieval algorithm, a priori information for aerosols and CO<sub>2</sub>, treatment of surface albedo, and the solar continuum model. Key updates to version 11 (v11) OCO-2 L2 products are the improvements made to the L1B processing, including gain degradation, noise model, footprint dependence, dispersion trend, and instrument line shape. Additionally, issues concerning the inadvertent flagging of most soundings over the South Atlantic Anomaly have been mitigated. V11 also includes several

spectroscopy updates and improvements to the ocean surface treatment, alongside the inclusion of new  $\text{CO}_2$  a priori profiles and minor changes to the rules governing sounding selection (Jacobs et al., 2024).

The transition from v11 to version 11.1 (v11.1) implements a new Digital Elevation Map (DEM) in the L2 retrievals that is used in the v11.1 “Lite” processing as a post-processing correction. The new DEM improves the retrievals at high latitudes, particularly above 60° N. Improving OCO-2 retrievals at high-latitude regions is necessary as the largest discrepancies among DEMs lie in these regions and warrant greater attention in the DEM quality assessment (Barlow et al., 2015; Byrne et al., 2020; Holland & Bitz, 2003; Jacobs et al., 2024; Pan et al., 2011; Park et al., 2018; Smith et al., 2019). The DEM used in the OCO ACOS algorithm (Zong, 2008; O’Dell et al., 2012) was updated for the first time since 2009 during the development of the OCO-2 ACOS retrieval algorithm for v11. Versions 10 and earlier used the OCODEM as the DEM (Osterman et al., 2020a, 2020b; Taylor et al., 2023). The v11.1 OCO-2 uses the Copernicus GLO90 DEM (hereafter referred to as the “Copernicus DEM”), a surface terrain model derived from the WorldDEM (Fahrland et al., 2020). Several studies have compared the performance of the Copernicus DEM to other DEMs (Bielski et al., 2024; Carrera-Hernandez, 2021; Guth & Geoffroy, 2021; Hachmeister et al., 2022; Karlson et al., 2021; Li et al., 2022). In a comprehensive global comparison of available DEMs for use in the OCO-2 ACOS retrieval algorithm, Jacobs et al. (2024) demonstrated that the Copernicus DEM is superior to other DEMs in terms of global continuity and accuracy and this motivated the post-processing update from OCO-2 v11 Lite files to v11.1 by substituting the NASADEM+ with the Copernicus DEM globally.

An important change in v11.1 is the modification of surface elevation, which changes the surface pressure. The most significant changes between v11 and v11.1 are observed at high latitudes due to the improved DEM accuracy. The change to the DEM, its impact on  $X_{\text{CO}_2}$ , and the bias correction of  $\text{co2\_ratio}$  and  $\text{h2o\_ratio}$  are described in detail by Jacobs et al. (2024). The v11.1 is a minor update to v11 that includes the following changes—modifications to “dP” (the difference between the retrieved and prior surface pressure) in the bias correction using the Copernicus DEM, the application of a bias correction to filter variables “ $\text{co2\_ratio}$ ” and “ $\text{h2o\_ratio}$ ” that are now replaced by “ $\text{co2\_ratio\_bc}$ ” and “ $\text{h2o\_ratio\_bc}$ ”, respectively, and updates related to quality filtering and bias corrections compared to v11.

In this analysis, we use the OCO-2 Level 2 (L2) release v11.1 “Lite” files, which are different from the L2 Standard products. The L2 Lite file data are daily files with additional post-processing data fields, including screened and bias-corrected  $X_{\text{CO}_2}$  values. The data in the Lite files are filtered using the  $\text{xco2\_quality\_flag}$ , where this variable, when set to “0,” indicates good quality soundings. All parameters used in the land and ocean bias correction, along with a detailed description of the overall bias correction process implemented in v11.1, are presented in the OCO-2 DUG ([https://docserver.gesdisc.eosdis.nasa.gov/public/project/OCO/OCO2\\_V11.1\\_OCO3\\_V10\\_L2\\_Data\\_Users\\_Guide\\_v3.0\\_RevA.pdf](https://docserver.gesdisc.eosdis.nasa.gov/public/project/OCO/OCO2_V11.1_OCO3_V10_L2_Data_Users_Guide_v3.0_RevA.pdf)).

The OCO-2 data record currently provides over a decade of  $X_{\text{CO}_2}$  observations. Thus, the possibility of drifts in the retrieved  $X_{\text{CO}_2}$  with time, such as those related to priors or calibration, could exist. To check for such spurious trends and account for averaging kernel effects, a linear least-square fit of the monthly mean of the  $X_{\text{CO}_2}$  difference of the OCO-2 and Truth data sets is performed. The process is described in detail in the OCO-2 DUG. The OCO-2 errors are treated as purely empirical as the analysis does not consider the possible drift in errors in TCCON or models. However, as the length of the OCO-2 data record grows, any spurious time trends should become easier to identify and eliminate. The current bias correction does not include a time-dependent term.

Atmospheric  $\text{CO}_2$  measurements are tied to primary standards governed by the National Oceanic and Atmospheric Administration (NOAA) Global Monitoring Laboratory. Revisions to the WMO  $\text{CO}_2$  calibration scale indicated increases in the  $\text{CO}_2$  mixing ratios on the order of 0.2 at 400 ppm (Hall et al., 2021; OCO-2 DUG, 2023). Since its finalization, in situ  $\text{CO}_2$  measurements are thus being recalibrated to this new scale, “WMO-CO2-X2019” (hereafter X2019). An additional variable, “ $\text{XCO2\_X2019}$ ,” is included in the OCO-2 v11.1 release that estimates the OCO-2  $X_{\text{CO}_2}$  on the X2019 scale. This was obtained by re-fitting the “ $\text{TCCON\_ADJUST}$ ” value from 0.9997 for the X2007 scale to 0.9995 for the X2019 scale, which resulted in an  $\sim 0.08$  ppm increase in  $X_{\text{CO}_2}$  values on the X2019 scale compared to the X2007 scale (OCO-2 DUG, 2023).

Table 1 provides a list of important updates to the ACOS L2FP retrieval algorithm spanning version 7 to version 11.2. Section 3 of O’Dell et al. (2018) discusses the ACOS retrieval algorithm updates that were made for v8 and compares them to previous versions. The v9  $X_{\text{CO}_2}$  product was an off-line reprocessing of the  $X_{\text{CO}_2}$  values

**Table 1**

*Key Updates to the ACOS L2 Full Physics (L2FP) Retrieval Algorithm for OCO-2 v7 Through v11.2*

		ACOS v7	ACOS v8/9	ACOS v10	ACOS v11	ACOS v11.1	ACOS v11.2
1	LiteCO <sub>2</sub> product release date	2015	2017/2018	2020	Aug-2022	June-2023	Oct-2024
2	Spectroscopy version	ABSCO v4.2	ABSCO v5.0 (Oyafuso et al., 2017)	ABSCO v5.1 (Payne et al., 2020)	ABSCO v5.2 (Payne et al., 2022)	No change	No change
3	Aerosol scheme	Gaussian profile for cloud-water, cloud-ice, and 2 aerosol types. Cloud-ice optical properties updated.	Monthly climatology from GMAO MERRA-2 for two dominant aerosol types. Stratospheric aerosol added to state vector	Daily GMAO GEOS5 FP-IT priors. Tightening of AOD prior variance. (Nelson & O'Dell, 2019)	No change	No change	No change
4	Meteorology prior source	ECMWF	GMAO GEOS5 FP-IT	No change	No change	No change	GMAO GEOS5 IT
5	CO <sub>2</sub> prior source	TCCON GGG2014 prior profiles with fixed secular increase	No change	TCCON GGG2020 prior profiles. Growth rate calculated from NOAA prior extrapolated after 2018.	Growth rate calculated from NOAA prior with approximately 1 month latency (Laughner et al., 2023)	No change	No change
6	Solar model	2016 Toon solar transmittance spectrum. ATLAS 3 SOLSPEC solar continuum.	No change	TSIS-SIM solar continuum	No change	No change	No change
7	Land surface parameterization	Pure Lambertian	Non-Lambertian BRDF model	No change	Corrected to use unpolarized RPV kernel	No change	No change
8	Water surface parameterization	Cox and Munk with additive Lambertian	No change	No change	Scaled Cox and Munk Error corrected in Stokes-U component.	No change	No change
9	Digital elevation model	OCODEM	No change	No change	NASADEM+ (Jacobs et al., 2024)	GLO-90 DEM (Jacobs et al., 2024)	No change
10	Global Bias against TCCON (ppm)	V7 OCO-2 <0.40 (absolute value across all modes, Wunch et al., 2017)	V9 OCO-2 LNG: -0.02 OG: -0.28 TG: 0.13	V10 OCO-2 LNG: 0.05 OG: 0.42 TG: 0.31	V11 OCO-2 LNG: -0.08 OG: 0.21 TG: 0.08	V11.1 OCO-2 LNG: -0.03 OG: 0.20 TG: -0.11	V11.2 OCO-2 LNG: 0.03 OG: 0.18 TG: -0.05

*Note.* LNG, OG, and TG indicate the Land Nadir/Glint, Ocean Glint, and Target modes, respectively. ECMWF and RPV stand for European Centre for Medium-Range Weather Forecasts, and Rahman Pinty Verstraete reflection model (Rahman et al., 1993), respectively. OCODEM is the DEM used for v10 and earlier OCO ACOS versions.

through the empirical bias correction and did not include any actual changes to the L2FP retrieval (Kiel et al., 2019). Section 3.1 of (Taylor et al., 2023) provides details for the v10 algorithm updates. A full discussion of the v11.1 digital elevation model is given by Jacobs et al. (2024), which also includes brief highlights of spectroscopy, CO<sub>2</sub> priors, and an update to the water surface parameterization in Appendix A. The most recent ACOS v11.2 was produced while the current work was under review. The update to the meteorological prior source was necessitated by a change in the GEOS5 FP product, which includes the addition of nitrate aerosols and adjustments to the essential meteorological parameters, for example, surface pressure and temperature profiles. A future publication by the OCO project will discuss this in detail. Extensive off-line testing indicated that the effect on global X<sub>CO<sub>2</sub></sub> is minimal, and v11.2 OCO-2 versus TCCON bias values have been briefly discussed in Section 3.

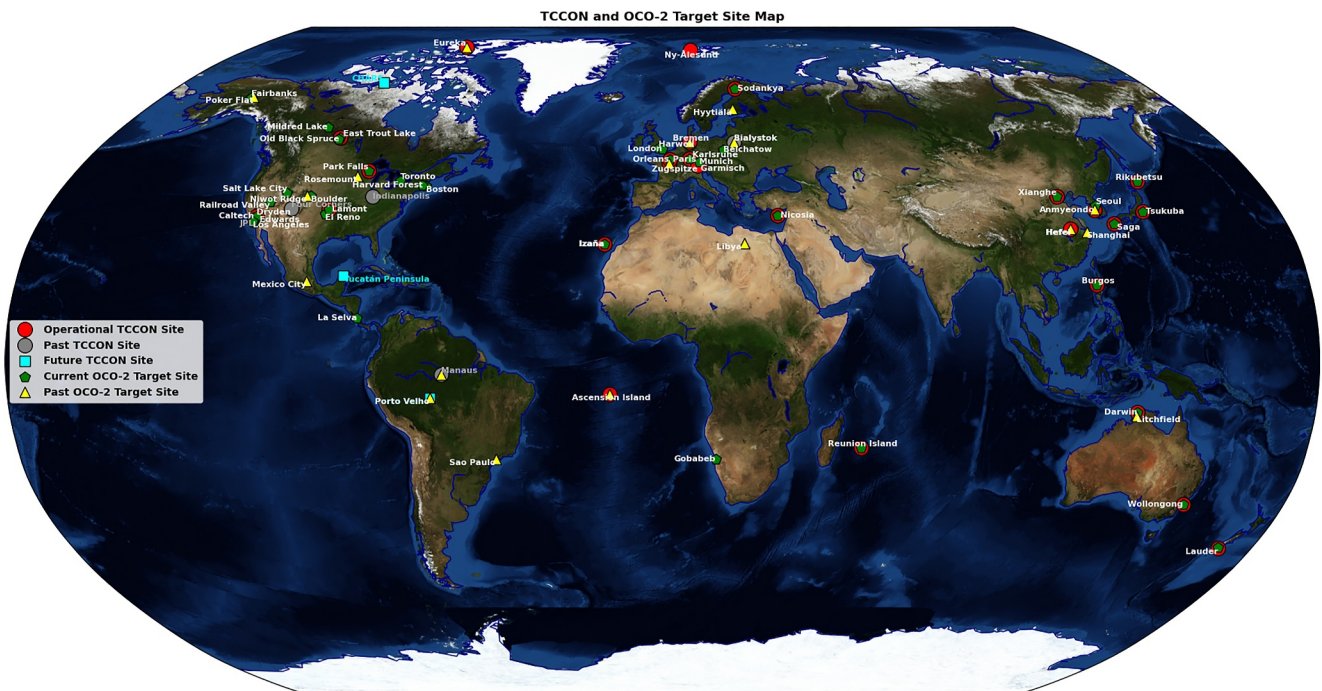


**Figure 1.** Map of all TCCON stations and OCO-2 target sites. Gray circles indicate previously operational sites, red circles indicate currently operational sites, and the cyan squares indicate future sites. Green pentagons show the current OCO-2 target locations, and the yellow triangles indicate the inactive OCO-2 target locations.

In addition to updates in the ACOS retrieval algorithm for each successive version, improvements were made to the L1b radiances through modifications to various calibration parameters. In addition, the empirical quality filtering and bias correction methodology, first described by Wunch, Wennberg, et al. (2011) and O'Dell et al. (2018), has continuously improved over time as both more training data has become available due to the longer OCO-2 time record, and due to improvements to the training data itself, especially with regard to TCCON updates (Laughner et al., 2024).

Although each version of the ACOS retrieval has shown decreases in Root Mean Square Error relative to truth metrics (TCCON, models, small area analysis), for example, Figure 1 in Taylor et al. (2023), there continue to be known sources of retrieval uncertainty, including, but not limited to, aerosols and spectroscopy (Bell et al., 2023; McGarragh et al., 2024).

### 2.1.2. TCCON

TCCON began operational measurements in 2004, with its first dedicated instrument located in Park Falls, WI, USA (Washenfelder et al., 2006; Wunch, Toon, et al., 2011; Wunch, Wennberg, et al., 2011). As of December 2023, the network has 29 sites across the globe and provides column average dry air mole fractions of CO<sub>2</sub> and other atmospheric species (X<sub>gas</sub>). These observations have been used to study natural and anthropogenic carbon fluxes (Babenhauserheide et al., 2020; Crowell et al., 2019; Dogniaux et al., 2021; Feng et al., 2017; Hedelius et al., 2018; Sussmann & Rettinger, 2020; Villalobos et al., 2021; Yang et al., 2007; Zhang et al., 2021), carbon transport (Keppel-Aleks et al., 2012; Polavarapu et al., 2016), to provide the ground truth values for space-based CO, CO<sub>2</sub>, and CH<sub>4</sub> measurements (Dupuy et al., 2016; Hedelius et al., 2019; Inoue et al., 2016; Jin et al., 2022; Kiel et al., 2019; Kulawik et al., 2016; Liang, Gong, et al., 2017; Liang, Gong, et al., 2017; Lorente et al., 2021; Schepers et al., 2016; Schneising et al., 2019; Sha et al., 2021; Velazco et al., 2019; Wunch et al., 2017; Yang et al., 2020), for model verification (Byrne et al., 2023), and to track long-term trends in column-average CO<sub>2</sub> (Yuan et al., 2019). The TCCON instruments measure solar absorption spectra in the NIR wavelengths and record an interferogram once every few minutes using solar-viewing high-resolution Fourier transform infrared spectrometers. The interferograms are processed using the GGG software suite to provide column average dry-air mole fractions. Note that GGG is not an acronym but the proper name of the software. Major GGG versions are indicated by the year of development. GGG2014 (Wunch et al., 2015) is the previous version used in the

generation of public TCCON data. Since GGG2014, GGG2020 is the most recent and first major update applied to public TCCON data. Detailed descriptions of the GGG2020 retrieval algorithm and the data version are provided by Laughner et al. (2024).

GGG2020 data is publicly available through the TCCON Data Archive ([tccondata.org](https://tccondata.org)). The publicly available TCCON data repository can be accessed through CaltechDATA (Total Carbon Column Observing Network (TCCON) Team, 2022). Documentation for the TCCON data product is available on the TCCON Wiki (<https://tccon-wiki.caltech.edu/>). The data use policy, and license are available at <https://tccon-wiki.caltech.edu/Main/DataUsePolicy>. Figure 1 shows a map of all inactive, currently operational, and future TCCON stations, indicated by gray circles, red circles, and cyan squares, respectively. This study uses TCCON data processed using GGG2020. Tables 2 and Table S1 in Supporting Information S1 include geographic locations and literature citations for the TCCON data sets used in this study.

## 2.2. OCO-2 Observation Modes

The nominal “science observation modes” for OCO-2 are the nadir and glint observation modes, alternating viewing by orbit except over the Atlantic and Pacific oceans. The nadir measurements are primarily useful only over land. The “glint” mode provides useful observations over both land and ocean surfaces. Different surface reflectance models are used in the ACOS full physics retrieval algorithm for land and ocean surfaces, and thus, the data in the glint mode are separated into glint over land (“land glint”) and ocean (“ocean glint”). The Lambertian surface reflectance model is used over land (matching the surface model of the nadir observation mode), and the Cox-Munk surface reflectance model with a Lambertian component is used over water (Wunch et al., 2017). Figure 2 shows the measurement density of OCO-2 in all modes as a function of latitude from September 2014 through December 2023. In the glint mode over the ocean, the retrievals are performed over a finite range of latitudes due to concerns arising from aerosol scattering-related biases over the most extensive optical path lengths. At high latitudes, the nadir mode provides reliable  $X_{CO_2}$  measurements over land. Over water bodies, such as inland lakes, data in the ocean glint mode are useful.

In the target mode, the OCO-2 satellite rotates from its nominal science mode during a target-mode maneuver to point at a selected ground location. During this time, the spacecraft’s solar panels are rotated away from the sun, and the spacecraft “dithers” (nods or scans) across the target site. The ground is swept across several times as the spacecraft passes overhead. During this time, several thousands of soundings are collected, a number of which are overlapped. This mode is primarily used for validation and calibration analysis. However, recently, target mode locations, such as Los Angeles, USA, and Belchatów, Poland, have been added for science analyses of large cities or in the vicinity of large power plants. The time to transition to and from the nominal science mode is  $\sim 5$  min each, and the target mode data are collected for  $\sim 4.5$  min during the ground sweep.

During the target-mode maneuvers, thousands of spectra are collected within 4.5 min over a target location, that is, a box  $\sim 0.2^\circ$  longitude  $\times 0.2^\circ$  latitude for the densest measurements. Tables 2 and Table S1 in Supporting Information S1 provide the current and past OCO-2 target locations, respectively. Note that the OCO-2 target list is periodically re-evaluated during the progress of the mission and is subject to updating in the future. Figure 1 shows the OCO-2 target sites, where the green pentagons indicate current target locations in 2025, and the yellow triangles indicate currently inactive target locations. The ground locations are required to be preprogrammed into the spacecraft software; thus, a limited number of sites (currently 38, increased from 19 at launch) can be targeted. Several OCO-2 target sites have been modified or replaced throughout the mission. The target locations are selected to cover a broad range of latitudes, longitudes, and surface properties that help identify existing biases that need to be corrected in the OCO-2 retrieval algorithm. The majority of these target-mode observations are made over TCCON sites. Those target locations have TCCON listed under the ‘Validation Data’ column in Tables 2 and Table S1 in Supporting Information S1 for the current and past sites, respectively. OCO-2 can target individual sites over specific orbits and only when the ground track is adequately close to the target site, thus allowing OCO-2 to choose from one to seven ground target locations. During each target maneuver, the associated power constraints thus limit the number of target observations that can be taken per day (maximum of four over a 24-hr period). Meteorological forecasts are considered before requesting target observations to maximize the chance of scenes without clouds. Another consideration is the number of targets selected at a specific location since the target observations mean the loss of the nadir or glint data for that orbit. This consideration allows for balance between target data with nadir and glint data and (for targets with a TCCON or other validation source)

**Table 2**  
*Current OCO-2 Targets*

Target name	Target location (Lat, lon)	Validation data	Target active dates	Data/Site reference
Belchatow, Poland	51.27, 19.33	Power Plant	Spring 2021–Present	Nassar et al. (2022)
Boston, Massachusetts, USA	42.38, -71.10	EM27/SUN, SIF	Spring 2021–Present	
Boulder, Colorado, USA	39.91, -104.24	AirCore, EM27/SUN	Spring 2015–Present	
Burgos, Philippines	18.5, 120.66	TCCON	January 2017–Present	Morino et al. (2022a)
Caltech, California, USA	34.12, -118.07	TCCON	July 2014–Present	Wennberg et al. (2022a)
Darwin, Australia	-12.37, 130.91	TCCON	July 2014–Present	Deutscher et al. (2023)
East Trout Lake, Saskatchewan, Canada	54.35, -104.98	TCCON	January 2017–Present	Wunch et al. (2022)
Edwards (Armstrong/Dryden), California, USA	34.95, -117.88	TCCON	July 2014–Present	Iraci et al. (2022)
El Reno, Oklahoma, USA	35.57, -98.06	SIF	March 2020–Present	
Fairbanks, Alaska, USA	64.85, -147.83	EM27/SUN	January 2017–Present	Jacobs et al. (2020)
Gobabeb, Namibia	-23.56, 15.04	EM27/SUN	Spring 2021–Present	Frey et al. (2021)
Harvard Forest, Massachusetts, USA	42.52, -72.17	EM27/SUN, SIF	Spring 2021–Present	
Harwell, England	51.57, -1.31	TCCON	Spring 2022–Present	Weidmann et al. (2023)
Izaña, Canary Islands, Spain	28.29, -16.51	TCCON	July 2014–Present	García et al. (2022)
Karlsruhe, Germany	49.10, 8.43	TCCON	July 2014–Present	Hase et al. (2023)
Lamont (ARM Southern Great Plains), Oklahoma, USA	36.60, -97.48	TCCON	July 2014–Present	Wennberg et al. (2022b)
La Selva, Costa Rica	10.43, -84.03	SIF	Spring 2022–Present	
Lauder, New Zealand	-45.00, 169.68	TCCON	July 2014–Present	Sherlock et al. (2022a, 2022b) Pollard et al. (2022)
London, England	51.52, -0.03	EM27/SUN	Spring 2022–Present	
Los Angeles, California, USA	33.81, -118.27	Megacity/EM27/SUN	January 2018–February 2019 Spring 2022–Present	
Mildred Lake, Alberta, Canada	57.03, -111.55	N/A	Spring 2021–Present	
Mexico City, Mexico	19.36, -99.16	EM27/SUN	Spring 2021–Present	
Munich, Germany	48.18, 11.51	EM27/SUN	March 2020–Present	
Nicosia, Cyprus	35.14, 33.38	TCCON	March 2020–Present	Petri et al. (2022)
Old Black Spruce, Saskatchewan, Canada	53.98, -105.12	SIF	February 2019–Present	
Paris, France	48.84, 2.35	TCCON	July 2014–Present	Té et al. (2022)
Park Falls, Wisconsin, USA	45.94, -90.27	TCCON	July 2014–Present	Wennberg et al. (2022c)
Railroad Valley, Nevada, USA	38.49, -115.69	Calibration	July 2014–Present	
Réunion Island, South Indian Ocean	-20.91, 55.51	TCCON	July 2014–Present	De Mazière et al. (2022)
Rikubetsu, Japan	43.45, 143.7	TCCON	Spring 2015–Present	Morino et al. (2022b)
Saga, Japan	33.24, 130.28	TCCON	Spring 2015–Present	Shiomi et al. (2022)
Salt Lake City, Utah, USA	40.71, -111.87	EM27/SUN	Spring 2022–Present	
Seoul, South Korea	37.52, 126.98	EM27/SUN	Spring 2021–Present	

**Table 2**  
*Continued*

Target name	Target location (Lat, lon)	Validation data	Target active dates	Data/Site reference
Sodankylä, Finland	67.36, 26.63	TCCON, AirCore, EM27/SUN	July 2014–Present	Kivi et al. (2022)
Toronto, Ontario, Canada	43.72, -79.43	EM27/SUN	March 2020–Present	
Tsukuba, Japan	36.05, 140.12	TCCON	July 2014–Present	Morino et al. (2022c)
Wollongong, Australia	-34.45, 150.85	TCCON	July 2014–Present	Deutscher et al. (2023)
Xianghe, China	39.80, 116.96	TCCON	Spring 2022–Present	Zhou et al. (2022)

*Note.* The target locations are stated in degrees latitude and degrees longitude. The list includes all current target locations, several of which are not TCCON sites. The target locations that have corresponding TCCON sites may not be absolutely centered on the TCCON site location. Targets that do not have corresponding TCCON sites are not discussed in the paper. SIF refers to Solar-Induced chlorophyll Fluorescence.

when validation data will be collected during the target. The retrieved  $X_{CO_2}$  is considered spatially and temporally constant within a target location (except for urban sites such as Caltech, Tsukuba, Paris, and Xianghe), given that most of these target sites are selected to be at a reasonable distance from large emission sources. Although  $X_{CO_2}$  in the atmosphere changes in only minor amounts over small geographic regions within  $\sim 4.5$  min, other parameters such as airmass (one airmass is the optical path length of one vertical column through the atmosphere), atmospheric path, albedo (surface reflectivity), and topography are subject to change in the duration of the maneuver. The retrieval algorithm aims to account for these changes and any unexpected variability in the target-mode measurements.

### 2.3. Coincidence Criteria

This section compares the bias-corrected OCO-2 land nadir/glint, ocean glint, and target mode data against the coincident TCCON data. The v11.1 OCO-2 “lite files” are bias-corrected using the three-step bias correction

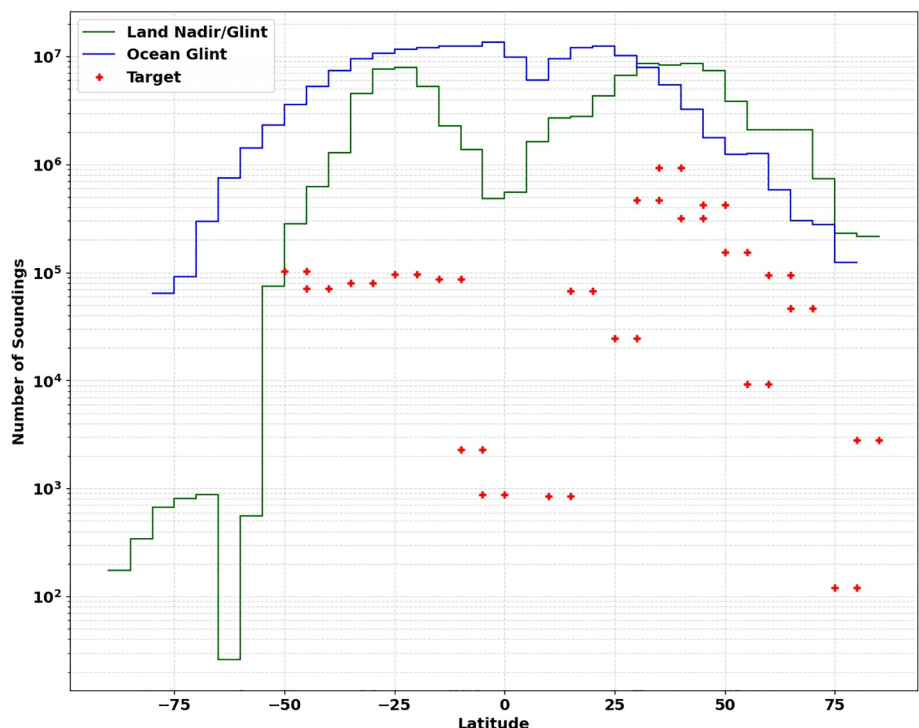


**Figure 2.** OCO-2 land nadir/glint, ocean glint, and target-mode measurement density from September 2014 to December 2023, plotted in  $5^\circ$  bins as a function of latitude using data from OCO-2 v11.1 “lite” files for “`xco2_quality_flag`” set to 0.

**Table 3**  
*Spatial Coincidence Criteria*

Site name	Observation mode	Latitude	Longitude
All sites except those listed below	All Modes	2.5°	5°
Caltech	Land Nadir/Glint	0.5°	0.5°
	Target	0.45° (not centered)	0.5°
Edwards	All Modes	1°	5°
Orléans	All Modes	1.5° (not centered)	5°
Paris	Land Nadir/Glint and Ocean Glint	2.5°	5°
	Target	1.7° (not centered)	5°
Tsukuba	All Modes	2.5°	1°

*Note.* The TCCON stations are centered within the coincidence boxes with the latitude and longitude values specified below. For some sites, over specific or all observation modes, the coincidence-box does not center on the TCCON station to eliminate redundant measurements originating from a particular side of the TCCON station. Those locations are indicated by “not centered.” Few sites use tighter spatial collocation in the target mode to exclude target mode observations from neighboring sites or the surrounding topography effect.

procedure described in the OCO-2 DUG. The data are then quality filtered, where only the good quality data are used by setting the “`xco2_quality_flag`” field to 0. The spatial coincidence criteria are listed in Table 3. A  $2.5^\circ \times 5^\circ$  latitude-longitude box centered on the TCCON site is used, where the box extends  $\pm 1.25^\circ$  in latitude and  $\pm 2.5^\circ$  in longitude from the TCCON site. The coincidence boxes are visually represented in the maps on the far right for each site in Figures S9 in Supporting Information S1 through Figure S34 in Supporting Information S1. Note that the spatial coincidence criteria used in this study are tighter than those used by Wunch et al. (2017), as the OCO-2 data are currently available for over a decade, with a high number of coincidences for each observation mode. Additionally, the use of tighter spatial coincidence requirements eliminates the possibility of overlaps between TCCON sites in close proximity to each other (e.g., Karlsruhe and Paris). The spatial coincidence area is reduced for specific polluted sites such as Caltech. For Edwards, this is done to eliminate the surface-elevation-induced biases (terrain effect). Slightly tighter spatial coincidence is also used for Orleans and Tsukuba compared to other sites. Median TCCON data within  $\pm 1$  hr of the OCO-2 overpass time are considered temporally coincident. As part of the coincidence criteria, a minimum of 100 good-quality OCO-2 soundings per overpass and at least 15 good-quality TCCON soundings within the temporal coincidence window are required. Furthermore, for all the TCCON data used in this analysis, following Wunch, Toon, et al. (2011), a correction was applied using the OCO-2 averaging kernels to convolve the TCCON  $X_{CO_2}$  with the OCO-2 column averaging kernel prior to comparing it with OCO-2  $X_{CO_2}$ . The application of the averaging kernels is necessary to adjust the  $X_{CO_2}$  values since the OCO-2 and TCCON  $X_{CO_2}$  retrievals were computed using slightly different a priori profiles. The retrievals must be computed about a common a priori profile, and the averaging kernel correction must account for the smoothing effect. This has been described in detail by Connor et al. (2008), Nguyen and Hobbs (2020), Rodgers and Connor (2003), and Wunch, Wennberg, et al. (2011).

### 3. Results and Discussion

#### 3.1. Land Nadir and Glint-Mode Comparisons to TCCON

Figure 3 compares the v11.1 OCO-2 bias corrected  $X_{CO_2}$  (`xco2_quality_flag` = 0) data in the land nadir/glint mode against the coincident TCCON data. The top left panel illustrates a one-to-one plot of the relationship between OCO-2  $X_{CO_2}$  and the median TCCON data during  $\pm 1$  hr of the OCO-2 overpass. “N” represents the number of coincident overpasses between OCO-2 and TCCON, “std” indicates the standard deviation, “ $r^2$ ” represents the coefficient of the determination, and the mean bias is represented by “bias.” The  $x$  and  $y$  axes indicate the TCCON and OCO-2  $X_{CO_2}$  values, respectively. The top right panel shows the frequency of the  $\Delta X_{CO_2}$  distribution. The  $x$ -axis shows the  $\Delta X_{CO_2}$  (OCO-2—TCCON) value, and the  $y$ -axis shows the frequency of occurrence. All  $X_{CO_2}$  and  $\Delta X_{CO_2}$  data are plotted in parts per million (ppm). In the bottom panel, the  $\Delta X_{CO_2}$  values are plotted as a time series, where the markers indicate the different sites. The  $x$ -axis indicates the year, and the  $y$ -axis shows the  $\Delta X_{CO_2}$  value. The sites are named in the upper portion of the panel, and the numbers within

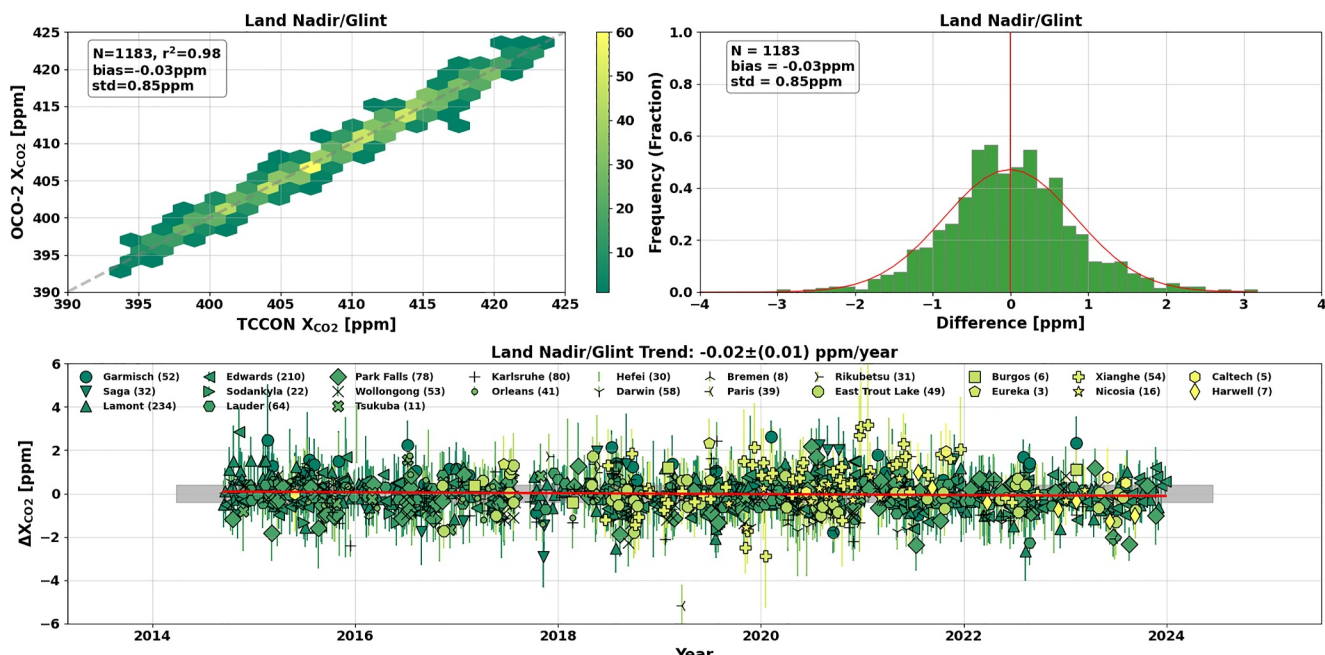


**Figure 3.** OCO-2 Land Nadir/Glint mode—(Top Left) The relation between each OCO-2 land nadir/glint mode observation's median value and the median value of the corresponding coincident TCCON data, recorded within  $\pm 1$  hr of the OCO-2 overpass. The one-to-one line is indicated by the dashed gray line. The number of coincident data points between OCO-2 and TCCON is indicated by “N”, the coefficient of determination is represented by “ $r^2$ ”, the bias is represented by “bias”, and the standard deviation is indicated by “std.” The x and y axes represent the  $X_{CO_2}$  data values in ppm for TCCON and OCO-2, respectively. Data are plotted as a “Hexbin plot”, where the color of each hexagonal bin indicates the number of points in it. (Top Right) The histogram provides the distribution of  $\Delta X_{CO_2}$  (OCO-2 minus TCCON). The x-axis shows the value of the difference and the y-axis indicates the fraction of observations. (Bottom) The time-series of  $\Delta X_{CO_2}$ . The markers indicate the different TCCON sites for which coincident OCO-2 data are available. The numbers within the parentheses indicate the N value for the corresponding TCCON station. The error bars indicate the standard deviation of  $\Delta X_{CO_2}$ . The solid red line indicates the time trend in ppm/year.

the parentheses next to a site indicate the number of coincidences between OCO-2 and TCCON for the corresponding site.

In the land nadir/glint modes, there are 1,183 coincident overpasses between OCO-2 and TCCON. The globally averaged bias is  $-0.03 \pm 0.85$  ppm. The small error observed is expected as the OCO-2 bias correction includes a term to minimize the difference. Using the updated DEM in the L2 retrievals primarily affected the retrievals above  $60^{\circ}\text{N}$  latitude. As the bottom panel indicates, the time series of  $\Delta X_{CO_2}$  values show a time trend of  $-0.02 \pm [0.01]$  ppm/year, calculated using a linear fit. This trend is statistically significant, and much of this trend is driven by a few sites (e.g., Darwin and Saga). Note that all reported time trends in this study are in the  $A \pm B$  ppm/year format, where A indicates the time trend, and B indicates the statistical uncertainty (standard error) in the time trend. In the top right panel, the distribution is centered very close to zero, and a comparable number of  $\Delta X_{CO_2}$  values lies on either side of the distribution. All bias-corrected and quality-filtered ( $xco2\_quality\_flag = 0$ ) OCO-2  $X_{CO_2}$  data compare better with coincident TCCON data at global scales in the land nadir/glint mode than earlier OCO-2 data versions. This indicates an improvement in the v11.1 land results as compared to a mean bias of  $0.05 \pm 0.84$  ppm for the v10 results (Figure S37 in Supporting Information S1). The latest v11.2 OCO-2 data, for a period comparable to v11.1 OCO-2 (September 2014 to March 2024), provides a similar comparison against TCCON, with a bias value of  $0.03 \pm 0.84$  ppm for  $N = 1,239$  in the land nadir/glint mode. The time trend of  $-0.01 \pm [0.01]$  ppm/year is not statistically significant.

### 3.2. Ocean Glint-Mode Comparisons to TCCON

Figure 4 compares the v11.1 OCO-2 data in the ocean glint mode against the coincident TCCON data and is plotted similarly to Figure 3. There are 328 coincidences between OCO-2 and TCCON for ocean glint, less than in the land nadir/glint and target modes, which is expected due to the limited number of TCCON sites near coastlines. The globally averaged bias in this mode is  $0.20 \pm 0.72$  ppm, with OCO-2 biased higher than the TCCON data. This is a factor of 10 higher bias than was seen for land nadir/glint collocations. However, compared to v10 results, there is a

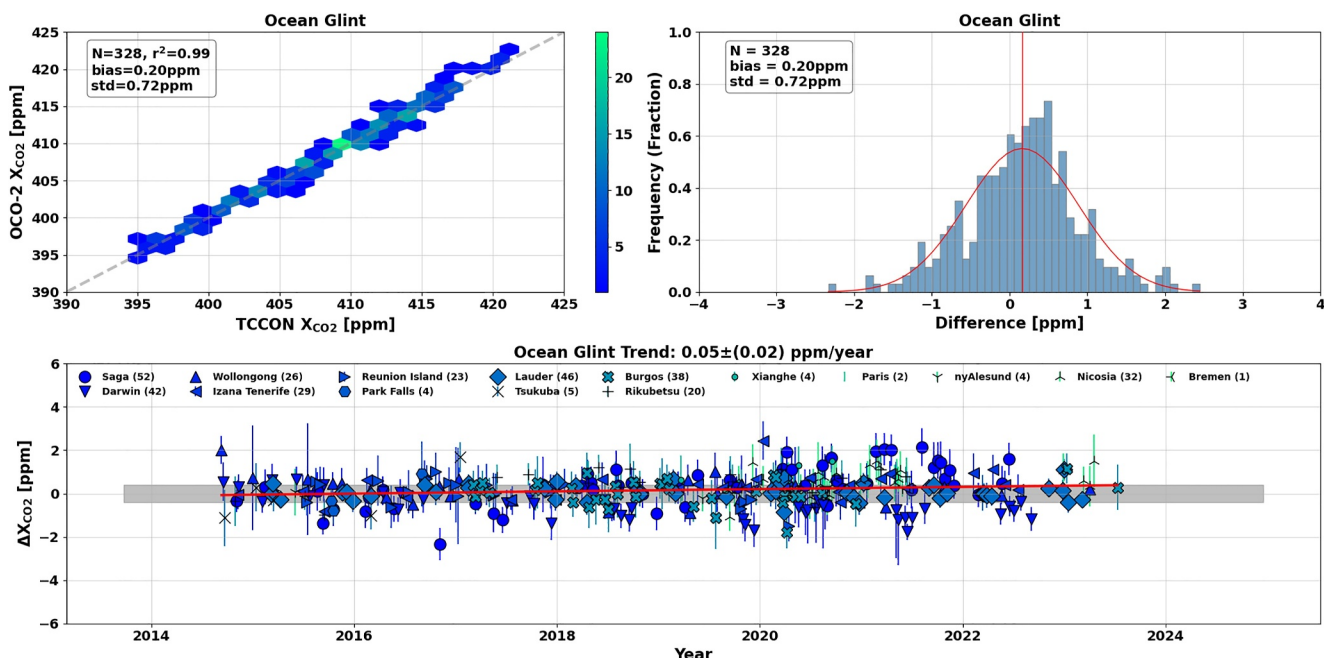


**Figure 4.** Same as Figure 3, but for the Ocean Glint mode of observation.

decrease in bias (Figure 9d in Taylor et al., 2023, and the middle panels in Figure S37 in Supporting Information S1) between OCO-2 and TCCON for ocean-glint due to the choice for v11 to determine the OCO-2 global scaling to match TCCON and not to the models (O'Dell et al., 2018; Section 3.3.1 in Taylor et al., 2023). Note that the standard deviation values for the ocean glint observations are lower than for the land nadir/glint and target mode observations. The v10 scaling against models introduced a bias of  $\sim 0.3$  ppm in the OCO-2  $X_{CO_2}$ . In v11, the ocean glint data are scaled using coastline crossings after scaling measurements over land to TCCON, which reduced the bias over the ocean in v11. This has reduced the bias and scatter over sites such as Bremen (with glint soundings in the North Sea), Ny Alesund (with glint soundings in the Arctic Ocean), and Park Falls (with glint soundings in the Great Lakes), for which higher bias values were reported in the earlier OCO-2 data versions (middle panels of Figure S35, S37, and S39 in Supporting Information S1 for v11, v10, and v9 OCO-2 vs. TCCON, respectively). The  $\Delta X_{CO_2}$  values show a time trend of  $0.05 \pm [0.02]$  ppm/year, which is statistically significant. The distribution in the top right panel indicates a higher number of positive than negative  $\Delta X_{CO_2}$  values. The aggregated bias-corrected OCO-2  $X_{CO_2}$  data, quality filtered with  $xco2\_quality\_flag = 0$  compared to coincident TCCON data, show a slightly higher global bias due to fewer coincidences and uncertainties than other observation modes. Furthermore, the collocation error is probably larger compared to land, and there is only a limited number of coastline crossings that can be used to derive the global scaling. The latest v11.2 OCO-2 data provides a similar comparison against TCCON, with a bias value of  $0.18 \pm 0.72$  ppm for  $N = 338$  in the ocean glint mode. The time trend of  $0.04 \pm [0.02]$  ppm/year is statistically significant.

### 3.3. Target-Mode Comparisons to TCCON

As discussed earlier, the measurements made in the target mode are used primarily for the bias correction of the OCO-2  $X_{CO_2}$  data, as they provide the most direct comparison, numerous collocations, and smaller collocation error relative to observations made in the nadir or glint mode. Figure 5 compares the v11.1 OCO-2 data in the target mode against the coincident TCCON data and is plotted akin to Figure 3. There is a total of 498 coincident target measurements between OCO-2 and TCCON. The globally averaged OCO-2 bias is  $-0.11 \pm 0.79$  ppm. There is a  $0.01 \pm [0.01]$  ppm/year trend in the  $\Delta X_{CO_2}$  data, which is not statistically significant. In the top right panel, although the distribution is centered close to zero, a higher number of  $\Delta X_{CO_2}$  values lies on the left side of the distribution. All bias-corrected and quality-filtered ( $xco2\_quality\_flag = 0$ ) OCO-2  $X_{CO_2}$  data compare well with coincident TCCON data in the target mode globally. The latest v11.2 OCO-2 data provides a similar

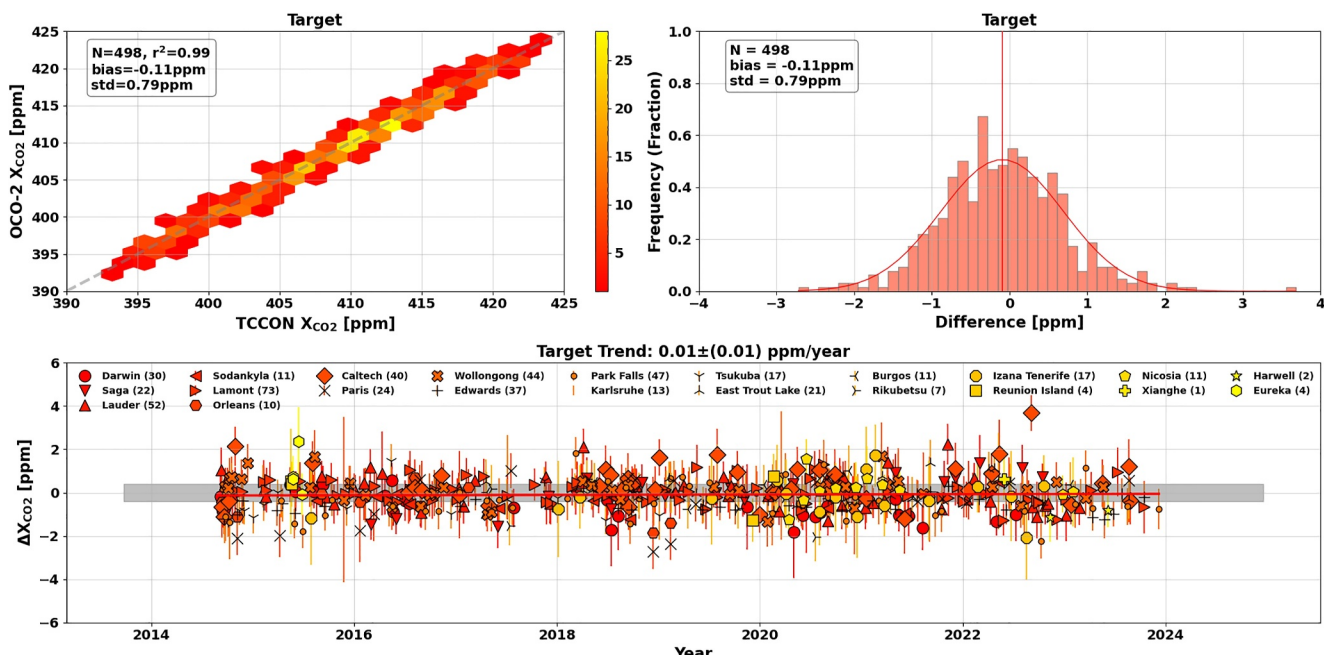


**Figure 5.** Same as Figure 3, but for the Target mode of observation.

comparison against TCCON, with a bias value of  $-0.05 \pm 0.81$  ppm for  $N = 516$  in the target mode. The time trend of  $0.00 \pm [0.01]$  ppm/year is not statistically significant.

Systematic biases are present in all current space-based measurements of CO<sub>2</sub> due to the uncertainties in the spectroscopy and oversimplification of atmosphere- and surface-related optical properties such as low-lying clouds, aerosols, and haze. Other biases can be introduced by the limited information content of measurements and issues related to instrument calibration (Crisp et al., 2017; Guerlet et al., 2013; Jacobs et al., 2024; Kiel et al., 2019; Schneising et al., 2012; Wunch, Toon, et al., 2011). To investigate further, we look at the target mode measurements in the one-to-one comparison in Figure 6 to identify TCCON sites and days with outlier points. Figure 6 shows the one-to-one relationship between the median value from each OCO-2 target mode observation and the median value of coincident TCCON data recorded within  $\pm 1$  hr of the OCO-2 overpass. The solid black line is the one-to-one line, and the dashed blue line indicates the best fit. This is the same data as presented in Figure 5 but shows individual collocations rather than hex-bin plots to identify outlier points and their corresponding TCCON sites. The numbers within the parentheses indicate the number of coincident measurements between OCO-2 and TCCON. A unique marker is used to indicate each TCCON site. While the v11.1 OCO-2 target mode data indicate excellent globally averaged bias against coincident TCCON data, there are specific outlier points for which the OCO-2 bias values are high ( $\sim > 2$  ppm). In Figure 6, most sites line up well on the one-to-one line. In Figure 7, in the top panel, we plot the magnitude of the sum in quadrature of the standard deviations of the OCO-2 target data (Wunch et al., 2017) and the coincident TCCON data. In the bottom panel, we plot those values as error bars, where the y-axis represents the OCO-2 X<sub>CO<sub>2</sub></sub>—Best Fit (from Figure 6) in ppm. Figures 6 and 7 indicate that the OCO-2 bias values are high over specific TCCON sites (e.g., Caltech, Lauder, and Wollongong). Since the v11.1 OCO-2 data are corrected for parameter-dependent and scaling biases, the residual biases over specific sites are possibly attributed to the surface properties and other uncertainties such as collocation error, spectroscopy, aerosol loading, and CO<sub>2</sub> enhancements or uptakes. Similar results have been seen in simulation studies specific to OCO-3 snapshot area mapping mode observations (Bell et al., 2023), which are directly applicable to OCO-2 target mode observations. In Section 3.5, we further investigate this by selecting sites with a significant number of coincident measurements between OCO-2 and TCCON.

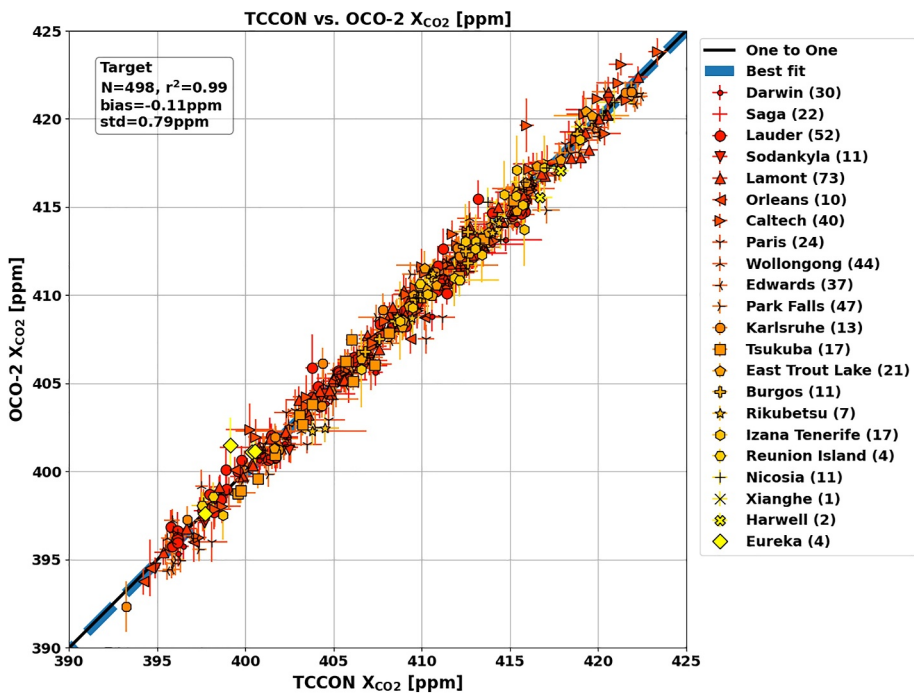


**Figure 6.** One-to-one plot indicating the relation between each OCO-2 target-mode maneuver's median value and the corresponding coincident TCCON data, recorded within  $\pm 1$  hr of the OCO-2 overpass. The solid black line is the one-to-one line and the dashed blue line indicates the best fit (linear fit). The numbers within the parentheses next to the TCCON site names indicate the number of coincident observations between OCO-2 and TCCON. The error bars indicate the standard deviation about the median.

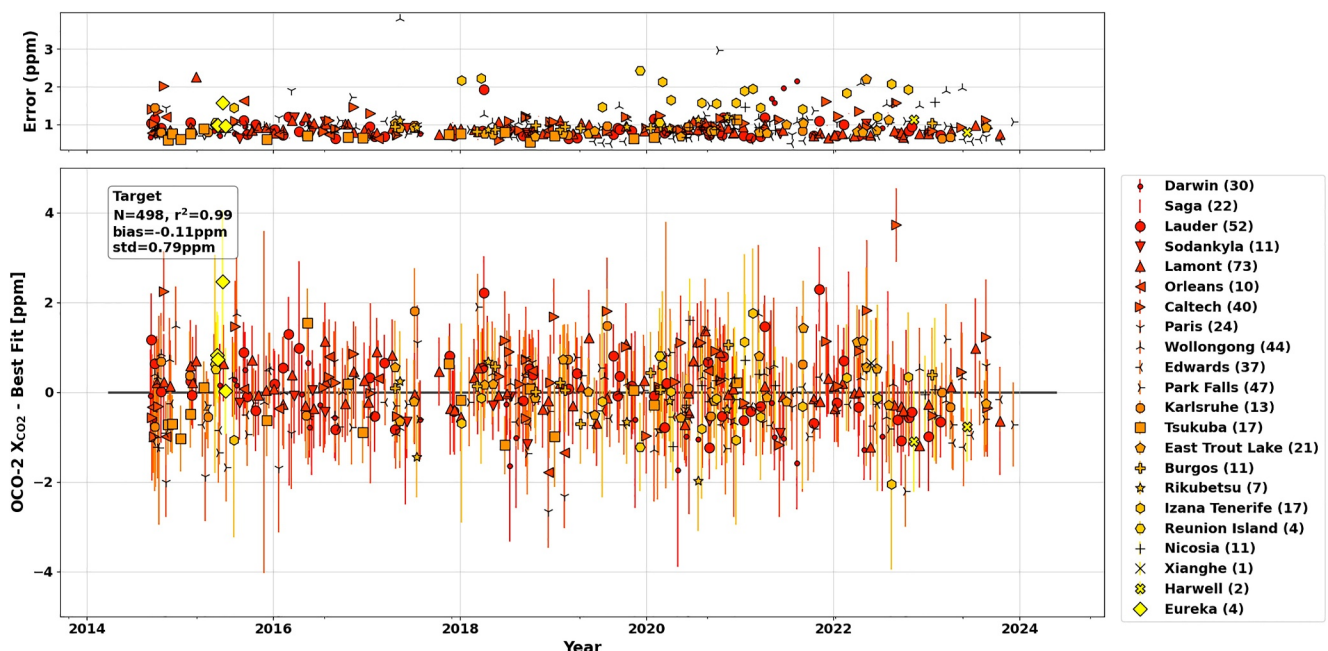


**Figure 7.** The differences between the OCO-2 target-data and the best fit line in Figure 6 plotted as a time series. The magnitude of the sum in quadrature of the standard deviation of the OCO-2 data in the target-mode and the standard deviation of the corresponding coincident TCCON data is indicated by the upper panel. In the bottom panel, those values are indicated as the error bars. The numbers within the parentheses next to the TCCON site names indicate the number of coincidences between OCO-2 and TCCON in the target-mode.

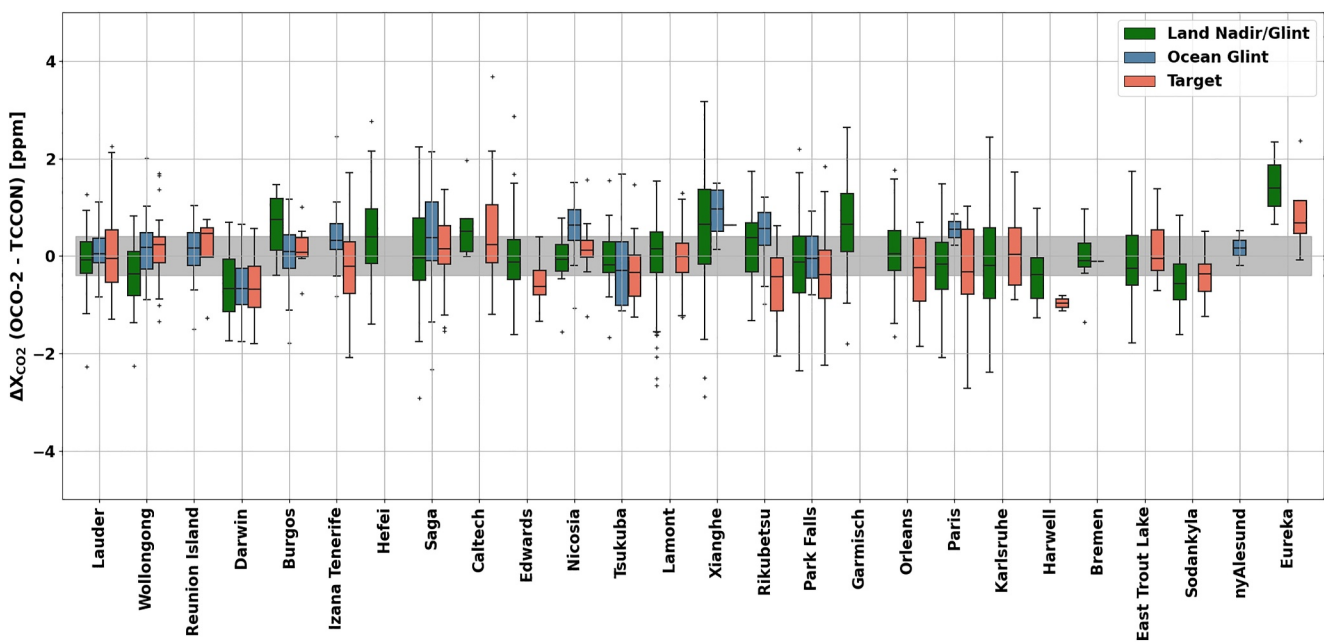


**Figure 8.** The observation mode-separated site-to-site  $\Delta X_{CO_2}$  values in ppm (OCO-2 minus corresponding coincident TCCON  $X_{CO_2}$  measurements). The bottom and top edges of the boxes indicate the 25 and 75 percentile limits, respectively. The whiskers show the full range of the data excluding outliers, and the outliers are shown by plus (“+”) symbols. The gray shaded area represents the  $\pm 0.4$  ppm uncertainty margin. Deviations beyond this shaded region are attributed more strongly to the uncertainties in the OCO-2 data.

### 3.4. Site-To-Site Differences

The site-to-site differences are shown in Figure 8. The sites are ordered by latitude from degrees South (far left) to degrees North (far right). The gray-shaded region represents the  $\pm 0.4$  ppm uncertainty in the TCCON  $X_{CO_2}$  values. The deviations beyond this range are attributable to the uncertainties in the OCO-2  $X_{CO_2}$  data (Wunch et al., 2017). The largest changes in the land nadir/glint mode of observation compared to OCO-2 v9, v10, and v11 (Figures S36, S38, and S40 in Supporting Information S1 for v11, v10, and v9 OCO-2 vs. TCCON, respectively) are seen in the high northern latitudes due to the change in the DEM. TCCON stations located in regions with large topographic variability (such as Lauder and Caltech) indicate  $\Delta X_{CO_2}$  values comparable to earlier OCO-2 data versions. In the ocean glint observation mode, there has been an overall decrease in the bias values compared to previous OCO-2 data versions due to the scaling against TCCON. Furthermore, there has been a reduction in the scatter due to the improved ocean surface treatment in v11.1. For the target mode observations, the most significant improvements have been at high-latitude sites such as Sodankylä due to the new DEM. There has been a decrease in the overall bias due to the updated global scaling factor. The seasonal variability in the  $\Delta X_{CO_2}$  data is shown in Figure S1 in Supporting Information S1.

### 3.5. OCO-2 Surface Properties Related Biases

In this section, we discuss the biases in the target mode associated with surface properties. The globally averaged target-mode OCO-2 biases against coincident TCCON data, shown in Figure 5, indicate good agreement. However, site-to-site differences exist between OCO-2 and TCCON, several of which are attributed to significant location-dependent biases. Wunch et al. (2017) suggest that differences with magnitudes within  $\pm 0.4$  ppm might be attributable to the TCCON station site-to-site biases, and this is consistent with the GGG2020 TCCON error budget (Laughner et al., 2024).

In this study, we investigate the differences between OCO-2 target mode observations and TCCON during specific days for the following sites - Edwards, Wollongong, Lauder, Nicosia, and Caltech, where site-specific biases are addressed. Several TCCON sites exist in regions with considerable spatial variability in ground cover or topography. Due to the impact of the local surface variability, target-mode observations over such regions are challenging for spaceborne  $X_{CO_2}$  retrievals. Earlier, GOSAT identified land surface property-related

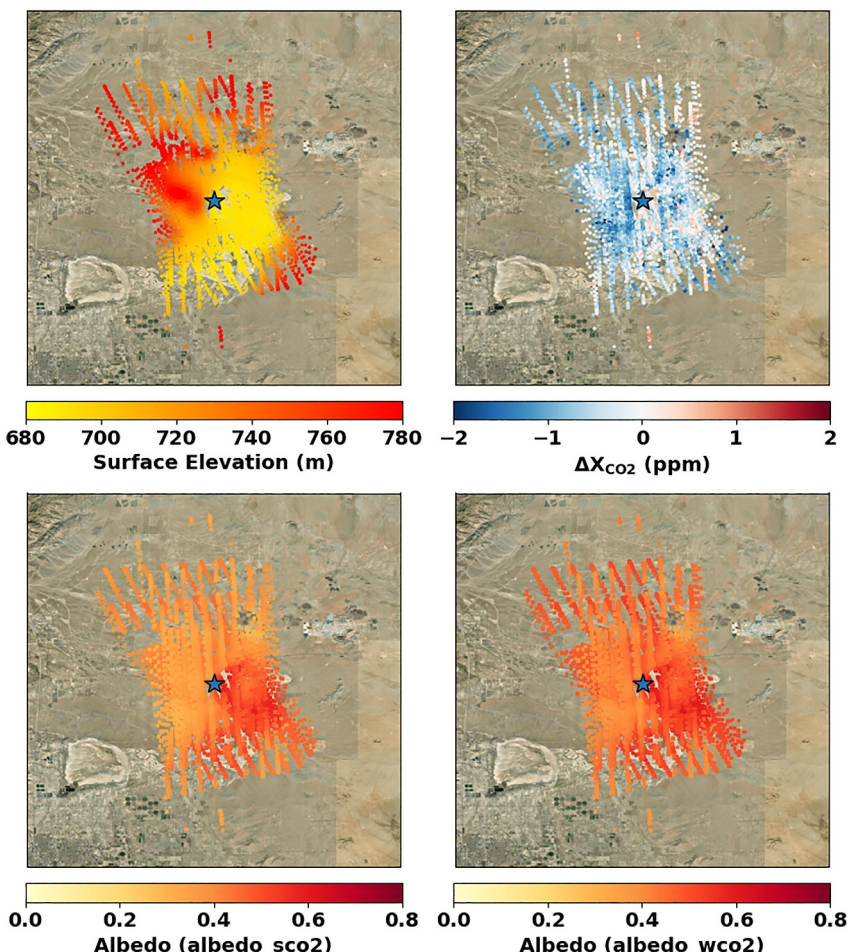


**Figure 9.** Target-mode measurements over Edwards. An ArcGIS image of the Edwards region is used as the background. The location of the Edwards TCCON station is indicated by the blue star. The top left panel indicates the surface elevation and the top right panel indicates the  $\Delta X_{\text{CO}_2}$  values in ppm (OCO-2 minus corresponding coincident TCCON  $X_{\text{CO}_2}$  measurements) on 19 April 2015. In this target-mode measurement, a surface brightness-related spatial bias is present. The bottom left and right panels indicate the OCO-2 albedo profiles for the strong and weak  $\text{CO}_2$  bands, respectively.

biases at the Edwards TCCON station, which is located in the bright California desert adjacent to a very bright playa with high NIR albedos and low topographic variability. Wunch et al. (2017) used OCO-2 v7 data to compare against coincident TCCON GGG2014 for the Edwards TCCON station and found that the OCO-2  $X_{\text{CO}_2}$  appeared to include a spurious dependence on surface brightness. Thus, higher OCO-2  $X_{\text{CO}_2}$  values were retrieved over brighter surfaces. Furthermore, they reported that the OCO-2  $X_{\text{CO}_2}$  data at Edwards is biased lower than the coincident TCCON  $X_{\text{CO}_2}$  for all target-mode observations averaged. Figure 7 from Wunch et al. (2017) for a target-mode observation over Edwards taken on 19 April 2015 indicates that  $\Delta X_{\text{CO}_2}$  values lie between  $\pm 5$  ppm. This figure has been recreated using the v11.1 OCO-2  $X_{\text{CO}_2}$  data and is shown in Figure 9. Note that we use different coincidence criteria than Wunch et al. (2017), as listed in Table 3, to evaluate the differences in  $X_{\text{CO}_2}$  data for this and all other sites. The spatial coincidence criteria are the same as those listed in Table 3. Median TCCON  $X_{\text{CO}_2}$  data within  $\pm 1$  hr of the OCO-2 overpass time are considered temporally coincident. In Figure 9, the top left panel indicates the elevation of the surface model, and the top right panel indicates the distribution of  $\Delta X_{\text{CO}_2}$ . The recreated plot indicates that for the same target-mode observation as Wunch et al. (2017), there has been a significant reduction in the magnitude of the bias, where  $\Delta X_{\text{CO}_2}$  values typically lie within  $\pm 2$  ppm. However, OCO-2 continues to report a low bias compared to coincident data, and for all mean target-mode  $X_{\text{CO}_2}$  at Edwards, OCO-2 is biased lower than the coincident TCCON  $X_{\text{CO}_2}$ , with a bias value of  $-0.62 \pm 0.41$  ppm. The bottom left and right panels indicate the albedo profiles of the strong and weak  $\text{CO}_2$  bands, respectively. High albedo is observed in both the strong and weak  $\text{CO}_2$  bands, with values typically  $>0.4$ .

**Table 4***Land Nadir/Glint, Ocean Glint, and Target Mode Statistics for Data Filtered Using the *xco2\_quality\_flag* = 0*

TCCON site	Land nadir/glint				Ocean glint				Target			
	Bias	Std dev	$R^2$	<i>N</i>	Bias	Std dev	$R^2$	<i>N</i>	Bias	Std dev	$R^2$	<i>N</i>
Bremen	-0.10	0.66	0.99	8	-0.12	-	-	1	-	-	-	-
Burgos	0.75	0.74	0.99	6	<b>0.09</b>	<b>0.58</b>	<b>0.98</b>	<b>38</b>	<b>0.07</b>	<b>0.44</b>	<b>0.98</b>	<b>11</b>
Caltech	0.51	0.79	0.99	5	-	-	-	-	<b>0.23</b>	<b>0.99</b>	<b>0.98</b>	<b>40</b>
Darwin	<b>-0.67</b>	<b>0.72</b>	<b>0.99</b>	<b>58</b>	<b>-0.66</b>	<b>0.60</b>	<b>0.99</b>	<b>42</b>	<b>-0.69</b>	<b>0.62</b>	<b>0.99</b>	<b>30</b>
East Trout Lake	<b>-0.26</b>	<b>0.75</b>	<b>0.98</b>	<b>49</b>	-	-	-	-	<b>-0.05</b>	<b>0.61</b>	<b>0.99</b>	<b>21</b>
Edwards	<b>-0.13</b>	<b>0.62</b>	<b>0.99</b>	<b>210</b>	-	-	-	-	<b>-0.62</b>	<b>0.41</b>	<b>1.00</b>	<b>37</b>
Eureka	1.39	0.85	0.10	3	-	-	-	-	0.68	1.04	0.69	4
Garmisch	<b>0.64</b>	<b>0.91</b>	<b>0.98</b>	<b>52</b>	-	-	-	-	-	-	-	-
Harwell	-0.39	0.77	0.96	7	-	-	-	-	-0.97	0.23	1.00	2
Hefei	<b>0.39</b>	<b>1.03</b>	<b>0.98</b>	<b>30</b>	-	-	-	-	-	-	-	-
Izana	-	-	-	-	<b>0.31</b>	<b>0.59</b>	<b>0.99</b>	<b>29</b>	<b>-0.21</b>	<b>0.89</b>	<b>0.97</b>	<b>17</b>
Karlsruhe	<b>-0.20</b>	<b>0.95</b>	<b>0.98</b>	<b>80</b>	-	-	-	-	<b>0.04</b>	<b>0.81</b>	<b>0.99</b>	<b>13</b>
Lamont	<b>0.15</b>	<b>0.70</b>	<b>0.99</b>	<b>234</b>	-	-	-	-	<b>-0.02</b>	<b>0.52</b>	<b>0.99</b>	<b>73</b>
Lauder	<b>-0.08</b>	<b>0.54</b>	<b>0.99</b>	<b>65</b>	<b>0.05</b>	<b>0.36</b>	<b>1.00</b>	<b>46</b>	<b>-0.05</b>	<b>0.77</b>	<b>0.99</b>	<b>52</b>
Nicosia	<b>-0.06</b>	<b>0.54</b>	<b>0.98</b>	<b>16</b>	<b>0.63</b>	<b>0.56</b>	<b>0.99</b>	<b>32</b>	<b>0.12</b>	<b>0.68</b>	<b>0.97</b>	<b>11</b>
NyAlesund	-	-	-	-	0.16	0.30	1.00	4	-	-	-	-
Orleans	<b>0.05</b>	<b>0.70</b>	<b>0.97</b>	<b>41</b>	-	-	-	-	-0.24	0.86	0.98	10
Paris	<b>-0.17</b>	<b>1.14</b>	<b>0.98</b>	<b>39</b>	0.54	0.46	1.00	2	<b>-0.33</b>	<b>1.10</b>	<b>0.97</b>	<b>24</b>
Park Falls	<b>-0.13</b>	<b>0.89</b>	<b>0.99</b>	<b>78</b>	<b>-0.05</b>	<b>0.74</b>	<b>0.98</b>	<b>4</b>	<b>-0.38</b>	<b>0.82</b>	<b>0.99</b>	<b>47</b>
Reunion Island	-	-	-	-	<b>0.16</b>	<b>0.57</b>	<b>0.98</b>	<b>23</b>	0.46	0.93	0.99	4
Rikubetsu	<b>0.38</b>	<b>0.77</b>	<b>0.99</b>	<b>31</b>	<b>0.56</b>	<b>0.61</b>	<b>0.99</b>	<b>20</b>	-0.43	0.93	0.98	7
Saga	<b>-0.04</b>	<b>1.19</b>	<b>0.97</b>	<b>32</b>	<b>0.38</b>	<b>0.96</b>	<b>0.98</b>	<b>52</b>	<b>0.15</b>	<b>0.78</b>	<b>0.99</b>	<b>22</b>
Sodankyla	<b>-0.57</b>	<b>0.60</b>	<b>0.99</b>	<b>22</b>	-	-	-	-	-0.36	0.48	1.00	<b>11</b>
Tsukuba	<b>-0.19</b>	<b>0.85</b>	<b>0.97</b>	<b>11</b>	-0.29	1.15	0.97	5	<b>-0.34</b>	<b>0.70</b>	<b>0.98</b>	<b>17</b>
Wollongong	<b>-0.37</b>	<b>0.61</b>	<b>0.99</b>	<b>53</b>	<b>0.18</b>	<b>0.63</b>	<b>0.99</b>	<b>26</b>	<b>0.23</b>	<b>0.61</b>	<b>0.99</b>	<b>44</b>
Xianghe	<b>0.64</b>	<b>1.28</b>	<b>0.90</b>	<b>54</b>	0.96	0.63	0.99	4	0.63	-	-	1
Total	<b>-0.03</b>	<b>0.85</b>	<b>0.98</b>	<b>1,183</b>	<b>0.20</b>	<b>0.72</b>	<b>0.99</b>	<b>328</b>	<b>-0.11</b>	<b>0.79</b>	<b>0.99</b>	<b>498</b>

*Note.* The bias (OCO-2 – TCCON), Standard deviation (Std Dev),  $R^2$ , and the number of coincidences (*N*) are listed below for each TCCON station. The results are marked in bold font for sites for which *N* > 10. All the coincidences in the table are considered independently to calculate the “Total” row.

(Bell et al., 2023). While the magnitudes of the bias values have reduced in v11.1 OCO-2 data, the results shown appear broadly consistent with the tendencies of those shown by Wunch et al. (2017). The results for Wollongong, Lauder, Nicosia, and Caltech are discussed in Supporting Information S1.

Table 4 compares the OCO-2 and coincident data in the land nadir/glint, ocean glint, and target modes. The aggregated bias-corrected and quality-filtered OCO-2 data, when compared to coincident TCCON data, indicate bias values of  $-0.03 \pm 0.85$ ,  $0.20 \pm 0.72$ , and  $-0.11 \pm 0.79$  ppm in the land nadir/glint, ocean glint, and target mode, respectively. For all comparisons for which *N* > 10, the mean-bias values range from  $-0.67 \pm 0.72$  ppm (Darwin) to  $0.64 \pm 1.28$  ppm (Xianghe) in the land nadir/glint mode,  $-0.66 \pm 0.60$  ppm (Darwin) to  $0.63 \pm 0.56$  ppm (Nicosia) in the ocean glint mode, and  $-0.69 \pm 0.62$  ppm (Darwin) to  $0.23 \pm 0.99$  ppm (Caltech) in the target mode. The correlation is identical for the ocean glint and target modes ( $R^2 = 0.99$ ) and comparable to the land nadir/glint mode ( $R^2 = 0.98$ ).

## 4. Conclusions

The aggregated bias-corrected and quality-filtered ( $xco2\_quality\_flag = 0$ ) OCO-2  $X_{CO_2}$  retrievals indicate improved agreement with the corresponding coincident TCCON data over all modes at global scales for the OCO-2 data version 11.1, compared to previous versions. In the land nadir/glint observation mode, the mean bias is  $-0.03 \pm 0.85$  ppm, and  $R^2$  is 0.98. In the ocean glint observation mode, the mean bias is  $0.20 \pm 0.72$  ppm, and the  $R^2$  value is 0.99. The mean bias in the target observation mode is  $-0.11 \pm 0.79$  ppm, and the  $R^2$  value is 0.99. The biases do not show a statistically significant time-dependent trend. Wunch et al. (2017) reported that latitude-dependent biases exist in the v7 OCO-2  $X_{CO_2}$  data version, with the highest biases apparent at latitudes poleward of  $45^\circ$ N. The implementation of the Copernicus DEM in v11.1 has partially remedied the bias at high latitudes, particularly those above  $60^\circ$  N, due to the improved accuracy in the DEM. The bias correction has significantly improved the relationship between the OCO-2 and TCCON globally, compared to older OCO-2 data versions. Furthermore, spurious  $X_{CO_2}$  variability attributed to the topography and surface brightness, evident in the target mode observations over Edwards (albedo), Wollongong (dark surface bias), and Lauder (surface elevation), reported previously by Wunch et al. (2017) for v7 has been significantly mitigated. While the nature of the current biases seen over these sites appears broadly consistent with the tendencies shown by Wunch et al. (2017), their overall magnitudes have significantly reduced in the v11.1 data version. The v11.1 OCO-2 data show improved agreement with TCCON over all modes and are better than the previous OCO-2 data versions. This study suggests that the new and improved v11.1 OCO-2  $X_{CO_2}$  data version is robust for use within the scientific community, but some precision and accuracy elements remain in the satellite  $X_{CO_2}$  estimates, which are likely attributable to retrieval errors driven by geometry, surface, and aerosol effects. The continued comparison of  $X_{CO_2}$  measurements from OCO-2 with TCCON over the land nadir/glint, ocean glint, and target modes of observation are crucial for monitoring and assessing the quality of the OCO-2  $X_{CO_2}$  data product.

## Data Availability Statement

OCO-2 Lite files are produced by the NASA OCO-2 project at the Jet Propulsion Laboratory, California Institute of Technology. The version 11.1 (v11.1) OCO-2 Lite files are available from NASA Goddard Earth Science Data and Information Services Center (GES-DISC): <https://daac.gsfc.nasa.gov/>, last access: 20 January 2025; DAAC, 2025). See OCO-2/OCO-3 Team/Vivienne Payne, Abhishek Chatterjee (2022) for v11.1 OCO-2 Lite files. TCCON data are available from the TCCON data archive, hosted by CaltechDATA (<https://tccondata.org/>, last access: 9 October 2024; TCCON Team, 2022). The references to data from individual TCCON sites are listed in Tables 2 and Table S1 in Supporting Information S1. All analyses were performed using Python 3.9.

## References

Babenhauserheide, A., Hase, F., & Morino, I. (2020). Net CO<sub>2</sub> fossil fuel emissions of Tokyo estimated directly from measurements of the Tsukuba TCCON site and radiosondes. *Atmospheric Measurement Techniques*, 13(5), 2697–2710. <https://doi.org/10.5194/amt-13-2697-2020>

Barlow, J. M., Palmer, P. I., Bruhwiler, L. M., & Tans, P. (2015). Analysis of CO<sub>2</sub> mole fraction data: First evidence of large-scale changes in CO<sub>2</sub> uptake at high northern latitudes. *Atmospheric Chemistry and Physics*, 15(23), 13739–13758. <https://doi.org/10.5194/acp-15-13739-2015>

Bell, E., O'Dell, C. W., Taylor, T. E., Merrelli, A., Nelson, R. R., Kiel, M., et al. (2023). Exploring bias in the OCO-3 snapshot area mapping mode via geometry, surface, and aerosol effects. *Atmospheric Measurement Techniques*, 16(1), 109–133. <https://doi.org/10.5194/amt-16-109-2023>

Bielski, C., López-Vázquez, C., Grohmann, C. H., Guth, P. L., Hawker, L., Gesch, D., et al. (2024). Novel approach for ranking DEMs: Copernicus DEM improves one arc second open global topography. *IEEE Transactions on Geoscience and Remote Sensing*, 62, 1–22. <https://doi.org/10.48550/arXiv.2302.08425>

Bovensmann, H., Burrows, J. P., Buchwitz, M., Frerick, J., Noel, S., Rozanov, V. V., et al. (1999). Sciamachy: Mission objectives and measurement modes. *Journal of the Atmospheric Sciences*, 56(2), 127–150. [https://doi.org/10.1175/1520-0469\(1999\)056<0127:SMOAMM>2.0.CO;2](https://doi.org/10.1175/1520-0469(1999)056<0127:SMOAMM>2.0.CO;2)

Byrne, B., Baker, D. F., Basu, S., Bertolacci, M., Bowman, K. W., Carroll, D., et al. (2022). National CO<sub>2</sub> budgets (2015–2020) inferred from atmospheric CO<sub>2</sub> observations in support of the global stocktake. *Earth System Science Data. Papers in Open Discussion*, 15, 1–59. <https://doi.org/10.5194/essd-2015-963-2023>

Byrne, B., Liu, J., Bowman, K., Pascolini-Campbell, M., Chatterjee, A., Pandey, S., et al. (2023). Unprecedented Canadian forest fire carbon emissions during 2023.

Byrne, B., Liu, J., Lee, M., Baker, I., Bowman, K. W., Deutscher, N. M., et al. (2020). Improved constraints on northern extratropical CO<sub>2</sub> fluxes obtained by combining surface-based and space-based atmospheric CO<sub>2</sub> measurements. *Journal of Geophysical Research: Atmospheres*, 125(15), e2019JD032029. <https://doi.org/10.1029/2019JD032029>

Carrera-Hernandez, J. J. (2021). Not all DEMs are equal: An evaluation of six globally available 30 m resolution DEMs with geodetic benchmarks and LiDAR in Mexico. *Remote Sensing of Environment*, 261, 112474. <https://doi.org/10.1016/j.rse.2021.112474>

Chevallier, F., Engelen, R. J., & Peylin, P. (2005). The contribution of AIRS data to the estimation of CO<sub>2</sub> sources and sinks. *Geophysical Research Letters*, 32(23), L23801. <https://doi.org/10.1029/2005GL024229>

Chevallier, F., Palmer, P. I., Feng, L., Boesch, H., O'Dell, C. W., & Bousquet, P. (2014). Toward robust and consistent regional CO<sub>2</sub> flux estimates from in situ and spaceborne measurements of atmospheric CO<sub>2</sub>. *Geophysical Research Letters*, 41(3), 1065–1070. <https://doi.org/10.1002/2013gl058772>

Connor, B. J., Boesch, H., Toon, G., Sen, B., Miller, C., & Crisp, D. (2008). Orbiting Carbon Observatory: Inverse method and prospective error analysis. *Journal of Geophysical Research*, 113(D5), D05305. <https://doi.org/10.1029/2006JD008336>

Crisp, D., Atlas, R. M., Breon, F. M., Brown, L. R., Burrows, J. P., Ciais, P., et al. (2004). The orbiting carbon observatory (OCO) mission. *Advances in Space Research*, 34(4), 700–709. <https://doi.org/10.1016/j.asr.2003.08.062>

Crisp, D., & Johnson, C. (2005). The orbiting carbon observatory mission. In *Acta Astronautica* (Vol. 56(1–2), pp. 193–197). Elsevier BV. <https://doi.org/10.1016/j.actaastro.2004.09.032>

Crisp, D., Miller, C. E., & DeCola, P. L. (2008). NASA orbiting carbon observatory: Measuring the column averaged carbon dioxide mole fraction from space. *Journal of Applied Remote Sensing*, 2(1), 023508. <https://doi.org/10.1117/1.2898457>

Crisp, D., Pollock, H. R., Rosenberg, R., Chapsky, L., Lee, R. A., Oyafuso, F. A., et al. (2017). The on-orbit performance of the Orbiting Carbon Observatory-2 (OCO-2) instrument and its radiometrically calibrated products. *Atmospheric Measurement Techniques*, 10(1), 59–81. <https://doi.org/10.5194/amt-10-59-2017>

Crowell, S., Baker, D., Schuh, A., Basu, S., Jacobson, A. R., Chevallier, F., et al. (2019). The 2015–2016 carbon cycle as seen from OCO-2 and the global in situ network. *Atmospheric Chemistry and Physics*, 19(15), 9797–9831. <https://doi.org/10.5194/acp-19-9797-2019>

De Mazière, M., Sha, M. K., Desmet, F., Hermans, C., Scialas, F., Kumps, N., et al. (2022). TCCON data from Réunion Island (RE), release GGG2020.R0 (version R0) [Dataset]. *CaltechDATA*. <https://doi.org/10.14291/TCCON.GGG2020.REUNION01.R0>

Deutscher, N. M., Griffith, D. W. T., Paton-Walsh, C., Velazco, V. A., Wennberg, P. O., Blavier, J.-F., et al. (2023). TCCON data from Darwin (AU), release GGG2020.R0 (version R0) [Dataset]. *CaltechDATA*. <https://doi.org/10.14291/TCCON.GGG2020.DARWIN01.R0>

Dogniaux, M., Crevoisier, C., Armante, R., Capelle, V., Delahaye, T., Cassé, V., et al. (2021). The Adaptable 4A Inversion (5AI): Description and first XCO<sub>2</sub> retrievals from orbiting carbon observatory-2 (OCO-2) observations. *Atmospheric Measurement Techniques*, 14(6), 4689–4706. <https://doi.org/10.5194/amt-14-4689-2021>

Dupuy, E., Morino, I., Deutscher, N. M., Yoshida, Y., Uchino, O., Connor, B. J., et al. (2016). Comparison of XH<sub>2</sub>O retrieved from GOSAT short-wavelength infrared spectra with observations from the TCCON network. *Remote Sensing*, 8(5), 414. <https://doi.org/10.3390/rs8050414>

Eldering, A., O'Dell, C. W., Wennberg, P. O., Crisp, D., Gunson, M. R., Viatte, C., et al. (2017). The orbiting carbon observatory-2: First 18 months of science data products. *Atmospheric Measurement Techniques*, 10(2), 549–563. <https://doi.org/10.5194/amt-10-549-2017>

Fahrlund, E., Jacob, P., Schrader, H., & Kahabka, H. (2020). *Copernicus digital elevation model product handbook*. Airbus Defence and Space—Intelligence. campaign ID: GEO.2018-1988-2RFP/RFI-No.: AO/1-9422/18/LG

Feng, L., Palmer, P. I., Bösch, H., Parker, R. J., Webb, A. J., Correia, C. S., et al. (2017). Consistent regional fluxes of CH 4 and CO 2 inferred from GOSAT proxy XCH 4: XCO 2 retrievals, 2010–2014. *Atmospheric Chemistry and Physics*, 17(7), 4781–4797. <https://doi.org/10.5194/acp-17-4781-2017>

Frey, M. M., Hase, F., Blumenstock, T., Dubravica, D., Groß, J., Götsche, F., et al. (2021). Long-term column-averaged greenhouse gas observations using a COCCON spectrometer at the high surface albedo site Gobabeb, Namibia. *Atmospheric Measurement Techniques Discussions*, 2021, 1–42.

García, O. E., Schneider, M., Herkommmer, B., Gross, J., Hase, F., Blumenstock, T., & Sepulveda, E. (2022). TCCON data from Izana (ES), release GGG2020.R1 (version R1) [Dataset]. *CaltechDATA*. <https://doi.org/10.14291/TCCON.GGG2020.IZANA01.R1>

Guerlet, S., Butz, A., Schepers, D., Basu, S., Hasekamp, O. P., Kuze, A., et al. (2013). Impact of aerosol and thin cirrus on retrieving and validating XCO<sub>2</sub> from GOSAT shortwave infrared measurements. *Journal of Geophysical Research: Atmospheres*, 118(10), 4887–4905. <https://doi.org/10.1002/jgrd.50332>

Guth, P. L., & Geoffroy, T. M. (2021). LiDAR point cloud and ICESat-2 evaluation of 1 second global digital elevation models: Copernicus wins. *Transactions in GIS*, 25(5), 2245–2261. <https://doi.org/10.1111/tgis.12825>

Hachmeister, J., Schneising, O., Buchwitz, M., Lorente, A., Borsdorff, T., Burrows, J. P., et al. (2022). On the influence of underlying elevation data on Sentinel-5 Precursor TROPOMI satellite methane retrievals over Greenland. *Atmospheric Measurement Techniques*, 15(13), 4063–4074. <https://doi.org/10.5194/amt-15-4063-2022>

Hall, B. D., Crotwell, A. M., Kitzis, D. R., Mefford, T., Miller, B. R., Schibig, M. F., & Tans, P. P. (2021). Revision of the world meteorological organization global atmosphere watch (WMO/GAW) CO 2 calibration scale. *Atmospheric Measurement Techniques*, 14(4), 3015–3032. <https://doi.org/10.5194/amt-14-3015-2021>

Hase, F., Herkommmer, B., Groß, J., Blumenstock, T., Kiel, M. ä., & Dohe, S. (2023). TCCON data from Karlsruhe (DE), release GGG2020.R1 (version R1) [Dataset]. *CaltechDATA*. <https://doi.org/10.14291/TCCON.GGG2020.KARLSRUHE01.R1>

Hedelius, J. K., He, T. L., Jones, D., Baier, B. C., Buchholz, R. R., De Mazière, M., et al. (2019). Evaluation of MOPITT Version 7 joint TIR–NIR X CO retrievals with TCCON. *Atmospheric Measurement Techniques*, 12(10), 5547–5572. <https://doi.org/10.5194/amt-12-5547-2019>

Hedelius, J. K., Liu, J., Oda, T., Maksyutov, S., Roehl, C. M., Iraci, L. T., et al. (2018). Southern California megacity CO 2, CH 4, and CO flux estimates using ground-and space-based remote sensing and a Lagrangian model. *Atmospheric Chemistry and Physics*, 18(22), 16271–16291. <https://doi.org/10.5194/acp-18-16271-2018>

Holland, M. M., & Bitz, C. M. (2003). Polar amplification of climate change in coupled models. *Climate Dynamics*, 21(3), 221–232. <https://doi.org/10.1007/s00382-003-0332-6>

Inoue, M., Morino, I., Uchino, O., Nakatsuru, T., Yoshida, Y., Yokota, T., et al. (2016). Bias corrections of GOSAT SWIR XCO 2 and XCH 4 with TCCON data and their evaluation using aircraft measurement data. *Atmospheric Measurement Techniques*, 9(8), 3491–3512. <https://doi.org/10.5194/amt-9-3491-2016>

Iraci, L. T., Podolske, J. R., Roehl, C., Wennberg, P. O., Blavier, J.-F., Allen, N., et al. (2022). TCCON data from Edwards (US), release GGG2020.R0 (version R0) [Dataset]. *CaltechDATA*. <https://doi.org/10.14291/TCCON.GGG2020.EDWARDS01.R0>

Jacobs, N., O'Dell, C. W., Taylor, T. E., Logan, T. L., Byrne, B., Kiel, M., et al. (2024). The importance of digital elevation model accuracy in X CO 2 retrievals: Improving the orbiting carbon observatory 2 atmospheric carbon observations from space version 11 retrieval product. *Atmospheric Measurement Techniques*, 17(5), 1375–1401. <https://doi.org/10.5194/amt-17-1375-2024>

Jacobs, N., Simpson, W. R., Wunch, D., O'Dell, C. W., Osterman, G. B., Hase, F., et al. (2020). Quality controls, bias, and seasonality of CO 2 columns in the boreal forest with orbiting carbon observatory-2: total carbon column observing network, and EM27/SUN measurements. *Atmospheric Measurement Techniques*, 13(9), 5033–5063. <https://doi.org/10.5194/amt-13-5033-2020>

Jin, C., Xue, Y., Jiang, X., Zhao, L., Yuan, T., Sun, Y., et al. (2022). A long-term global XCO<sub>2</sub> dataset: Ensemble of satellite products. *Atmospheric Research*, 279, 106385. <https://doi.org/10.1016/j.atmosres.2022.106385>

Karlsson, M., Bastviken, D., & Reese, H. (2021). Error characteristics of pan-arctic digital elevation models and elevation derivatives in Northern Sweden. *Remote Sensing*, 13(22), 4653. <https://doi.org/10.3390/rs13224653>

Keppel-Aleks, G., Toon, G. C., Wennberg, P. O., & Deutscher, N. M. (2007). Reducing the impact of source brightness fluctuations on spectra obtained by Fourier-transform spectrometry. *Applied Optics*, 46(21), 4774–4779. <https://doi.org/10.1364/AO.46.004774>

Keppel-Aleks, G., Wennberg, P. O., & Schneider, T. (2011). Sources of variations in total column carbon dioxide. *Atmospheric Chemistry and Physics*, 11(8), 3581–3593. <https://doi.org/10.5194/acp-11-3581-2011>

Keppel-Aleks, G., Wennberg, P. O., Washenfelder, R. A., Wunch, D., Schneider, T., Toon, G. C., et al. (2012). The imprint of surface fluxes and transport on variations in total column carbon dioxide. *Biogeosciences*, 9(3), 875–891. <https://doi.org/10.5194/bg-9-875-2012>

Kiel, M., O'Dell, C. W., Fisher, B., Eldering, A., Nassar, R., MacDonald, C. G., & Wennberg, P. O. (2019). How bias correction goes wrong: Measurement of X CO<sub>2</sub> affected by erroneous surface pressure estimates. *Atmospheric Measurement Techniques*, 12(4), 2241–2259. <https://doi.org/10.5194/amt-12-2241-2019>

Kivi, R., & Heikkilä, P. (2016). Fourier transform spectrometer measurements of column CO<sub>2</sub> at Sodankylä, Finland. *Geoscientific Instrumentation, Methods and Data Systems*, 5(2), 271–279. <https://doi.org/10.5194/gi-5-271-2016>

Kivi, R., Heikkilä, P., & Kyrö, E. (2022). TCCON data from Sodankylä (FI), release GGG2020.R0 (version R0) [Dataset]. *CaltechDATA*. <https://doi.org/10.14291/TCCON.GGG2020.SODANKYLA01.R0>

Kulawik, S., Wunch, D., O'Dell, C., Frankenberg, C., Reuter, M., Oda, T., et al. (2016). Consistent evaluation of ACOS-GOSAT, BESD-SCIAMACHY, CarbonTracker, and MACC through comparisons to TCCON. *Atmospheric Measurement Techniques*, 9(2), 683–709. <https://doi.org/10.5194/amt-9-683-2016>

Kuze, A., Suto, H., Nakajima, M., & Hamazaki, T. (2009). Thermal and near infrared sensor for carbon observation Fourier-transform spectrometer on the Greenhouse Gases Observing Satellite for greenhouse gases monitoring. *Applied Optics*, 48(35), 6716–6733. <https://doi.org/10.1364/AO.48.006716>

Kuze, A., Suto, H., Shiomi, K., Kawakami, S., Tanaka, M., Ueda, Y., et al. (2016). Update on GOSAT TANSO-FTS performance, operations, and data products after more than 6 years in space. *Atmospheric Measurement Techniques*, 9(6), 2445–2461. <https://doi.org/10.5194/amt-9-2445-2016>

Laughner, J. L., Roche, S., Kiel, M., Toon, G. C., Wunch, D., Baier, B. C., et al. (2023). A new algorithm to generate a priori trace gas profiles for the GGG2020 retrieval algorithm. *Atmospheric Measurement Techniques*, 16(5), 1121–1146. <https://doi.org/10.5194/amt-16-1121-2023>

Laughner, J. L., Toon, G. C., Mendonça, J., Petri, C., Roche, S., Wunch, D., et al. (2024). The total carbon column observing network's GGG2020 data version. *Earth System Science Data*, 16(5), 2197–2260. <https://doi.org/10.5194/essd-16-2197-2024>

Li, H., Zhao, J., Yan, B., Yue, L., & Wang, L. (2022). Global DEMs vary from one to another: An evaluation of newly released Copernicus, NASA and AW3D30 DEM on selected terrains of China using ICESat-2 altimetry data. *International Journal of Digital Earth*, 15(1), 1149–1168. <https://doi.org/10.1080/17538947.2022.2094002>

Liang, A., Gong, W., Han, G., & Xiang, C. (2017). Comparison of satellite-observed XCO<sub>2</sub> from GOSAT, OCO-2, and ground-based TCCON. *Remote Sensing*, 9(10), 1033. <https://doi.org/10.3390/rs9101033>

Liang, A., Han, G., Gong, W., Yang, J., & Xiang, C. (2017). Comparison of global XCO<sub>2</sub> concentrations from OCO-2 with tccon data in terms of latitude zones. *Ieee Journal of Selected Topics in Applied Earth Observations and Remote Sensing*, 10(6), 2491–2498. <https://doi.org/10.1109/jstas.2017.2650942>

Liu, Y., Wang, J., Yao, L., Chen, X., Cai, Z., Yang, D., et al. (2018). The TanSat mission: Preliminary global observations. *Science Bulletin*, 63(18), 1200–1207. <https://doi.org/10.1016/j.scib.2018.08.004>

Lorente, A., Borsdorff, T., Butz, A., Hasekamp, O., Aan De Brugh, J., Schneider, A., et al. (2021). Methane retrieved from TROPOMI: Improvement of the data product and validation of the first 2 years of measurements. *Atmospheric Measurement Techniques*, 14(1), 665–684. <https://doi.org/10.5194/amt-14-665-2021>

Mandrake, L., O'Dell, C. W., Wunch, D., Wennberg, P. O., Fisher, B., Osterman, G. B., & Eldering, A. (2015). *Orbiting Carbon Observatory-2 (OCO-2) Warm Level, Bias Correction, and Lite File Product Description*. Jet Propulsion Laboratory. California Institute of Technology, Pasadena Retrieved from [http://disc.sci.gsfc.nasa.gov/OCO-2/documentation/oco-2-v7/OCO2\\_XCO2\\_Lite\\_Files\\_and\\_Bias\\_Correction\\_0915\\_sm.pdf](http://disc.sci.gsfc.nasa.gov/OCO-2/documentation/oco-2-v7/OCO2_XCO2_Lite_Files_and_Bias_Correction_0915_sm.pdf)

McGarragh, G. R., O'Dell, C. W., Crowell, S. M., Somkuti, P., Burgh, E. B., & Moore, I. I. B. (2024). The GeoCarb greenhouse gas retrieval algorithm: Simulations and sensitivity to sources of uncertainty. *Atmospheric Measurement Techniques*, 17(3), 1091–1121. <https://doi.org/10.5194/amt-17-1091-2024>

Messerschmidt, J., Geibel, M. C., Blumenstock, T., Chen, H., Deutscher, N. M., Engel, A., et al. (2011). Calibration of TCCON column-averaged CO<sub>2</sub>: The first aircraft campaign over European TCCON sites. *Atmospheric Chemistry and Physics*, 11(21), 10765–10777. <https://doi.org/10.5194/acp-11-10765-2011>

Miller, C. E., Crisp, D., DeCola, P. L., Olsen, S. C., Randerson, J. T., Michalak, A. M., et al. (2007). Precision requirements for space-based data. *Journal of Geophysical Research*, 112(D10), D10314. <https://doi.org/10.1029/2006JD007659>

Morino, I., Ohyama, H., Hori, A., & Ikegami, H. (2022b). TCCON data from Rikubetsu (JP), release GGG2020.R0 (version R0) [Dataset]. *CaltechDATA*. <https://doi.org/10.14291/TCCON.GGG2020.RIKUBETSU01.R0>

Morino, I., Ohyama, H., Hori, A., & Ikegami, H. (2022c). TCCON data from Tsukuba (JP), 125HR, release GGG2020.R0 (version R0) [Dataset]. *CaltechDATA*. <https://doi.org/10.14291/TCCON.GGG2020.TSUKUBA02.R0>

Morino, I., Velasco, V. A., Hori, A., Uchino, O., & Griffith, D. W. T. (2022a). TCCON data from Burgos, Ilocos Norte (PH), release GGG2020. R0 (version R0) [Dataset]. *CaltechDATA*. <https://doi.org/10.14291/TCCON.GGG2020.BURGOS01.R0>

Nassar, R., Moeini, O., Mastrogiacomo, J. P., O'Dell, C. W., Nelson, R. R., Kiel, M., et al. (2022). Tracking CO<sub>2</sub> emission reductions from space: A case study at Europe's largest fossil fuel power plant. *Frontiers in Remote Sensing*, 3, 1028240. <https://doi.org/10.3389/frsen.2022.1028240>

Nelson, R. R., & O'Dell, C. W. (2019). The impact of improved aerosol priors on near-infrared measurements of carbon dioxide. *Atmospheric Measurement Techniques*, 12(3), 1495–1512. <https://doi.org/10.5194/amt-12-1495-2019>

Nguyen, H., & Hobbs, J. (2020). Intercomparison of remote sensing retrievals: An Examination of prior-induced biases in averaging kernel corrections. *Remote Sensing*, 12(19), 3239. <https://doi.org/10.3390/rs12193239>

O'Dell, C. W., Connor, B., Bösch, H., O'Brien, D., Frankenberg, C., Castano, R., et al. (2012). The ACOS CO<sub>2</sub> retrieval algorithm—Part 1: Description and validation against synthetic observations. *Atmospheric Measurement Techniques*, 5(1), 99–121. <https://doi.org/10.5194/amt-5-99-2012>

O'Dell, C. W., Eldering, A., Wennberg, P. O., Crisp, D., Gunson, M. R., Fisher, B., et al. (2018). Improved retrievals of carbon dioxide from Orbiting Carbon Observatory-2 with the version 8 ACOS algorithm. *Atmospheric Measurement Techniques*, 11(12), 6539–6576. <https://doi.org/10.5194/amt-11-6539-2018>

Osterman, G., O'Dell, C., Eldering, A., Fisher, B., Crisp, D., Cheng, C., et al. (2020a). Data product user's Guide. *Operational Level 2 Data Versions 10 and Lite File Version 10 and VEarly*. [https://docserver.gesdisc.eosdis.nasa.gov/public/project/OCO/OCO2\\_OCO3\\_B10\\_DUG.pdf](https://docserver.gesdisc.eosdis.nasa.gov/public/project/OCO/OCO2_OCO3_B10_DUG.pdf)

Osterman, G., O'Dell, C., Eldering, A., Fisher, B., Crisp, D., Cheng, C., et al. (2020b). *Orbiting carbon observatory-2 & 3 (OCO-2 & OCO-3) data product user's guide, operational level 2 data versions 10 and lite file version 10 and yearly*. National Aeronautics and Space

Administration Jet Propulsion Laboratory California Institute of Technology Pasadena. Retrieved from [https://docserver.gesdisc.eosdis.nasa.gov/public/project/OCO/OCO2\\_OCO3\\_B10\\_DUG.pdf](https://docserver.gesdisc.eosdis.nasa.gov/public/project/OCO/OCO2_OCO3_B10_DUG.pdf) 22 July 2023.

Oyafuso, F., Payne, V. H., Drouin, B. J., Devi, V. M., Benner, D. C., Sung, K., et al. (2017). High accuracy absorption coefficients for the Orbiting Carbon Observatory-2 (OCO-2) mission: Validation of updated carbon dioxide cross-sections using atmospheric spectra. *Journal of Quantitative Spectroscopy and Radiative Transfer*, 203, 213–223. <https://doi.org/10.1016/j.jqsrt.2017.06.012>

Pan, Y., Birdsey, R. A., Fang, J., Houghton, R., Kauppi, P. E., Kurz, W. A., et al. (2011). A large and persistent carbon sink in the world's forests. *Science*, 333(6045), 988–993. <https://doi.org/10.1126/science.1201609>

Park, K., Kang, S. M., Kim, D., Stuecker, M. F., & Jin, F. F. (2018). Contrasting local and remote impacts of surface heating on polar warming and amplification. *Journal of Climate*, 31(8), 3155–3166. <https://doi.org/10.1175/JCLI-D-17-0600.1>

Payne, V., Chatterjee, A., Rosenberg, R., Kiel, M., Fisher, B., Dang, L., et al. (2022). Data product user's Guide, operational level 2 lite files: L2Std, L2 lite OCO-2 v11 and OCO-3 v10/10.4. [https://docserver.gesdisc.eosdis.nasa.gov/public/project/OCO/OCO2\\_V11\\_OCO3\\_V10\\_DUG.pdf](https://docserver.gesdisc.eosdis.nasa.gov/public/project/OCO/OCO2_V11_OCO3_V10_DUG.pdf) (last access: 14 June 2023).

Payne, V. H., Drouin, B. J., Oyafuso, F., Kuai, L., Fisher, B. M., Sung, K., et al. (2020). Absorption coefficient (ABSCO) tables for the orbiting carbon observatories: Version 5.1. *Journal of Quantitative Spectroscopy and Radiative Transfer*, 255, 107217. <https://doi.org/10.1016/j.jqsrt.2020.107217>

Petri, C., Vrekoussis, M., Rousogenous, C., Warneke, T., Sciare, J., & Notholt, J. (2022). TCCON data from Nicosia (CY), release GGG2020.R0 (version R0) [Dataset]. *CaltechDATA*. <https://doi.org/10.14291/TCCON.GGG2020.NICOSIA01.R0>

Polavarapu, S. M., Neish, M., Tanguay, M., Girard, C., de Grandpre, J., Semeniuk, K., et al. (2016). Greenhouse gas simulations with a coupled meteorological and transport model: The predictability of CO 2. *Atmospheric Chemistry and Physics*, 16(18), 12005–12038. <https://doi.org/10.5194/acp-16-12005-2016>

Pollard, D. F., Robinson, J., & Shiona, H. (2022). TCCON data from lauder (NZ), release GGG2020.R0 (version R0) [Dataset]. *CaltechDATA*. <https://doi.org/10.14291/TCCON.GGG2020.LAUDER03.R0>

Rahman, H., Pinty, B., & Verstraete, M. M. (1993). Coupled surface-atmosphere reflectance (CSAR) model: 2. Semiempirical surface model usable with NOAA advanced very high resolution radiometer data. *Journal of Geophysical Research*, 98(D11), 20791–20801. <https://doi.org/10.1029/93JD02072>

Rayner, P. J., & O'Brien, D. M. (2001). The utility of remotely sensed CO2 concentration data in surface source inversions. *Geophysical Research Letters*, 28(1), 175–178. <https://doi.org/10.1029/2000GL011912>

Rodgers, C. D., & Connor, B. J. (2003). Intercomparison of remote sounding instruments. *Journal of Geophysical Research*, 108(D3), 4116. <https://doi.org/10.1029/2002jd002299>

Schepers, D., Butz, A., Hu, H., Hasekamp, O. P., Arnold, S. G., Schneider, M., et al. (2016). Methane and carbon dioxide total column retrievals from cloudy GOSAT soundings over the oceans. *Journal of Geophysical Research: Atmospheres*, 121(9), 5031–5050. <https://doi.org/10.1002/2015jd023389>

Schneising, O., Bergamaschi, P., Bovensmann, H., Buchwitz, M., Burrows, J. P., Deutscher, N. M., et al. (2012). Atmospheric greenhouse gases retrieved from SCIAMACHY: Comparison to ground-based FTS measurements and model results. *Atmospheric Chemistry and Physics*, 12(3), 1527–1540. <https://doi.org/10.5194/acp-12-1527-2012>

Schneising, O., Buchwitz, M., Reuter, M., Bovensmann, H., Burrows, J. P., Borsdorff, T., et al. (2019). A scientific algorithm to simultaneously retrieve carbon monoxide and methane from TROPOMI onboard Sentinel-5 Precursor. *Atmospheric Measurement Techniques*, 12(12), 6771–6802. <https://doi.org/10.5194/amt-12-6771-2019>

Sha, M. K., Langerock, B., Blavier, J. F. L., Blumenstock, T., Borsdorff, T., Buschmann, M., et al. (2021). Validation of methane and carbon monoxide from Sentinel-5 Precursor using TCCON and NDACC-IRWG stations. *Atmospheric Measurement Techniques Discussions*, 2021, 1–84. <https://doi.org/10.5194/amt-14-6249-2021>

Sherlock, V., Connor, B., Robinson, J., Shiona, H., Smale, D., & Pollard, D. F. (2022a). TCCON data from lauder (NZ), 120HR, release GGG2020.R0 (version R0) [Dataset]. *CaltechDATA*. <https://doi.org/10.14291/TCCON.GGG2020.LAUDER01.R0>

Sherlock, V., Connor, B., Robinson, J., Shiona, H., Smale, D., & Pollard, D. F. (2022b). TCCON data from Lauder (NZ), 125HR, release GGG2020.R0 (version R0) [Dataset]. *CaltechDATA*. <https://doi.org/10.14291/TCCON.GGG2020.LAUDER02.R0>

Shiomi, K., Kawakami, S., Ohyama, H., Arai, K., Okumura, H., Ikegami, H., & Usami, M. (2022). TCCON data from Saga (JP), release GGG2020.R0 (version R0) [Dataset]. *CaltechDATA*. <https://doi.org/10.14291/TCCON.GGG2020.SAGA01.R0>

Smith, D. M., Screen, J. A., Deser, C., Cohen, J., Fyfe, J. C., García-Serrano, J., et al. (2019). The polar amplification model intercomparison project (PAMIP) contribution to CMIP6: Investigating the causes and consequences of polar amplification. *Geoscientific Model Development*, 12(3), 1139–1164. <https://doi.org/10.5194/gmd-12-1139-2019>

Strong, K., Roche, S., Franklin, J. E., Mendonca, J., Lutsch, E., Weaver, D., et al. (2022). TCCON data from Eureka (CA), release GGG2020.R0 (version R0) [Dataset]. *CaltechDATA*. <https://doi.org/10.14291/TCCON.GGG2020.EUREKA01.R0>

Sussmann, R., & Rettinger, M. (2020). Can we measure a COVID-19-related slowdown in atmospheric CO2 growth? Sensitivity of total carbon column observations. *Remote Sensing*, 12(15), 2387. <https://doi.org/10.3390/rs12152387>

Taylor, T. E., O'Dell, C. W., Baker, D., Bruegge, C., Chang, A., Chapsky, L., et al. (2023). Evaluating the consistency between OCO-2 and OCO-3 XCO2 estimates derived from the NASA ACOS version 10 retrieval algorithm. *Atmospheric Measurement Techniques*, 16(12), 3173–3209. <https://doi.org/10.5194/amt-2022-329>

Taylor, T. E., O'Dell, C. W., Baker, D., Bruegge, C., Chang, A., Chapsky, L., et al. (2023). Evaluating the consistency between OCO-2 and OCO-3 XCO2 estimates derived from the NASA ACOS version 10 retrieval algorithm. *Atmospheric Measurement Techniques Discussions*, 2023, 1–61.

Té, Y., Jeseck, P., & Janssen, C. (2022). TCCON data from Paris (FR), release GGG2020.R0 (version R0) [Dataset]. *CaltechDATA*. <https://doi.org/10.14291/TCCON.GGG2020.PARIS01.R0>

Toon, G., Blavier, J. F., Washenfelder, R., Wunch, D., Keppel-Aleks, G., Wennberg, P., et al. (2009). Total column carbon observing network (TCCON). In *Hyperspectral imaging and Sensing of the environment*. Optica Publishing Group. <https://doi.org/10.1364/FTS.2009.JMA3>

Velazco, V. A., Deutscher, N. M., Morino, I., Uchino, O., Bukosa, B., Ajiro, M., et al. (2019). Satellite and ground-based measurements of XCO 2 in a remote semiarid region of Australia. *Earth System Science Data*, 11(3), 935–946. <https://doi.org/10.5194/essd-11-935-2019>

Villalobos, Y., Rayner, P. J., Silver, J. D., Thomas, S., Haverd, V., Knauer, J., et al. (2021). Was Australia a sink or source of CO 2 in 2015? Data assimilation using OCO-2 satellite measurements. *Atmospheric Chemistry and Physics*, 21(23), 17453–17494. <https://doi.org/10.5194/acp-21-17453-2021>

Washenfelder, R. A., Toon, G. C., Blavier, J. F., Yang, Z., Allen, N. T., Wennberg, P. O., et al. (2006). Carbon dioxide column abundances at the Wisconsin Tall Tower site. *Journal of Geophysical Research*, 111(D22), D22305. <https://doi.org/10.1029/2006JD007154>

Weidmann, D., Brownsword, R., & Doniki, S. (2023). TCCON data from Harwell, Oxfordshire (UK), release GGG2020.R0 (version R0) [Dataset]. *CaltechDATA*. <https://doi.org/10.14291/TCCON.GGG2020.HARWELL01.R0>

Wennberg, P. O., Roehl, C. M., Wunch, D., Blavier, J.-F., Toon, G. C., Allen, N. T., et al. (2022a). TCCON data from Caltech (US), release GGG2020.R0 (version R0) [Dataset]. *CaltechDATA*. <https://doi.org/10.14291/TCCON.GGG2020.PASADENA01.R0>

Wennberg, P. O., Roehl, C. M., Wunch, D., Toon, G. C., Blavier, J.-F., Washenfelder, R., et al. (2022c). TCCON data from Park Falls (US), release GGG2020.R1 (version R1) [Dataset]. *CaltechDATA*. <https://doi.org/10.14291/tccon.ggg2020.parkfalls01.R1>

Wennberg, P. O., Wunch, D., Roehl, C. M., Blavier, J.-F., Toon, G. C., & Allen, N. T. (2022b). TCCON data from Lamont (US), release GGG2020.R0 (version R0) [Dataset]. *CaltechDATA*. <https://doi.org/10.14291/TCCON.GGG2020.LAMONT01.R0>

Wunch, D., Mendonca, J., Colebatch, O., Allen, N. T., Blavier, J.-F., Kunz, K., et al. (2022). TCCON data from East Trout lake, SK (CA), release GGG2020.R0 (version R0) [Dataset]. *CaltechDATA*. <https://doi.org/10.14291/tccon.ggg2020.eastroutlake01.R0>

Wunch, D., Toon, G. C., Blavier, J. F. L., Washenfelder, R. A., Notholt, J., Connor, B. J., et al. (2011). The total carbon column observing network. *Philosophical Transactions of the Royal Society A: Mathematical, Physical and Engineering Sciences*, 369(1943), 2087–2112. <https://doi.org/10.1098/rsta.2010.0240>

Wunch, D., Toon, G. C., Sherlock, V., Deutscher, N. M., Liu, C., Feist, D. G., & Wennberg, P. O. (2015). Documentation for the 2014 TCCON data release. *Tech. rep.*, *CaltechDATA*. <https://doi.org/10.14291/TCCON.GGG2014.DOCUMENTATION.R0/1221662>

Wunch, D., Toon, G. C., Wennberg, P. O., Wofsy, S. C., Stephens, B. B., Fischer, M. L., et al. (2010). Calibration of the total carbon column observing network using aircraft profile data. *Atmospheric Measurement Techniques*, 3(5), 1351–1362. <https://doi.org/10.5194/amt-3-1351-2010>

Wunch, D., Wennberg, P. O., Osterman, G., Fisher, B., Naylor, B., Roehl, C. M., et al. (2017). Comparisons of the orbiting carbon observatory-2 (OCO-2) X CO 2 measurements with TCCON. *Atmospheric Measurement Techniques*, 10(6), 2209–2238. <https://doi.org/10.5194/amt-10-2209-2017>

Wunch, D., Wennberg, P. O., Toon, G. C., Connor, B. J., Fisher, B., Osterman, G. B., et al. (2011). A method for evaluating bias in global measurements of CO 2 total columns from space. *Atmospheric Chemistry and Physics*, 11(23), 12317–12337. <https://doi.org/10.5194/acp-11-12317-2011>

Yang, D., Boesch, H., Liu, Y., Somkuti, P., Cai, Z., Chen, X., et al. (2020). Toward high precision XCO2 retrievals from TanSat observations: Retrieval improvement and validation against TCCON measurements. *Journal of Geophysical Research: Atmospheres*, 125(22), e2020JD032794. <https://doi.org/10.1029/2020JD032794>

Yang, Z. R. A. W., Washenfelder, R. A., Keppel-Aleks, G., Krakauer, N. Y., Randerson, J. T., Tans, P. P., et al. (2007). New constraints on Northern Hemisphere growing season net flux. *Geophysical Research Letters*, 34(12), L12807. <https://doi.org/10.1029/2007GL029742>

Yuan, Y., Sussmann, R., Rettig, M., Ries, L., Petermeier, H., & Menzel, A. (2019). Comparison of continuous in-situ CO2 measurements with co-located column-averaged XCO2 TCCON/satellite observations and carbontracker model over the Zugspitze region. *Remote Sensing*, 11(24), 2981. <https://doi.org/10.3390/rs11242981>

Zhang, Y., Jacob, D. J., Lu, X., Maasakkers, J. D., Scarpelli, T. R., Sheng, J. X., et al. (2021). Attribution of the accelerating increase in atmospheric methane during 2010–2018 by inverse analysis of GOSAT observations. *Atmospheric Chemistry and Physics*, 21(5), 3643–3666. <https://doi.org/10.5194/acp-21-3643-2021>

Zhou, M., Wang, P., Kumps, N., Hermans, C., & Nan, W. (2022). TCCON data from Xianghe, China, release GGG2020.R0 (version R0) [Dataset]. *CaltechDATA*. <https://doi.org/10.14291/tccon.ggg2020.xianghe01.R0>

Zong, J. (2008). Application of global high-resolution DEM in the OCO mission. *International Archives of the Photogrammetry, Remote Sensing, and Spatial Information Sciences*, 37, XXXVII.

## References From the Supporting Information

Deutscher, N. M., Notholt, J., Messerschmidt, J., Weinzierl, C., Warneke, T., Petri, C., & Grupe, P. (2019). TCCON data from Bialystok (PL), release GGG2014.R2 (version R2) [Dataset]. *CaltechDATA*. <https://doi.org/10.14291/TCCON.GGG2014.BIALYSTOK01.R2>

Dubey, M. K., Henderson, B. G., Allen, N. T., Blavier, J.-F., Roehl, C. M., & Wunch, D. (2022). TCCON data from Manaus (BR), release GGG2020.R0 (version R0) [Dataset]. *CaltechDATA*. <https://doi.org/10.14291/TCCON.GGG2020.MANAUS01.R0>

Feist, D. G., Arnold, S. G., John, N., & Geibel, M. C. (2017). TCCON data from Ascension Island (SH), release GGG2014.R0 (GGG2014.R0) [Dataset]. *CaltechDATA*. <https://doi.org/10.14291/TCCON.GGG2014.ASCENSION01.R0/1149285>

Goo, T.-Y., Oh, Y.-S., & Velasco, V. A. (2014). TCCON data from Anmyeondo (KR), release GGG2014.R0 (GGG2014.R0) [Dataset]. *CaltechDATA*. <https://doi.org/10.14291/TCCON.GGG2014.ANMEYONDO01.R0/1149284>

Liu, C., Wang, W., Sun, Y., & Shan, C. (2023). TCCON data from Hefei (PRC), release GGG2020.R1 (version R1) [Dataset]. *CaltechDATA*. <https://doi.org/10.14291/TCCON.GGG2020.HEFEI01.R1>

Massie, S. T., Cronk, H., Merrelli, A., O'Dell, C., Schmidt, K. S., Chen, H., & Baker, D. (2021). Analysis of 3D cloud effects in OCO-2 XCO2 retrievals. *Atmospheric Measurement Techniques*, 14(2), 1475–1499. <https://doi.org/10.5194/amt-14-1475-2021>

Notholt, J., Petri, C., Warneke, T., & Buschmann, M. (2022). TCCON data from Bremen (DE), release GGG2020.R0 (version R0) [Dataset]. *CaltechDATA*. <https://doi.org/10.14291/TCCON.GGG2020.BREMEN01.R0>

Warneke, T., Petri, C., Notholt, J., & Buschmann, M. (2022). TCCON data from Orléans (FR), release GGG2020.R0 (version R0) [Dataset]. *CaltechDATA*. <https://doi.org/10.14291/tccon.ggg2020.orleans01.R0>